iScience

Article

Hepatic iNKT cells facilitate colorectal cancer metastasis by inducing a fibrotic niche in the liver

Graphical abstract

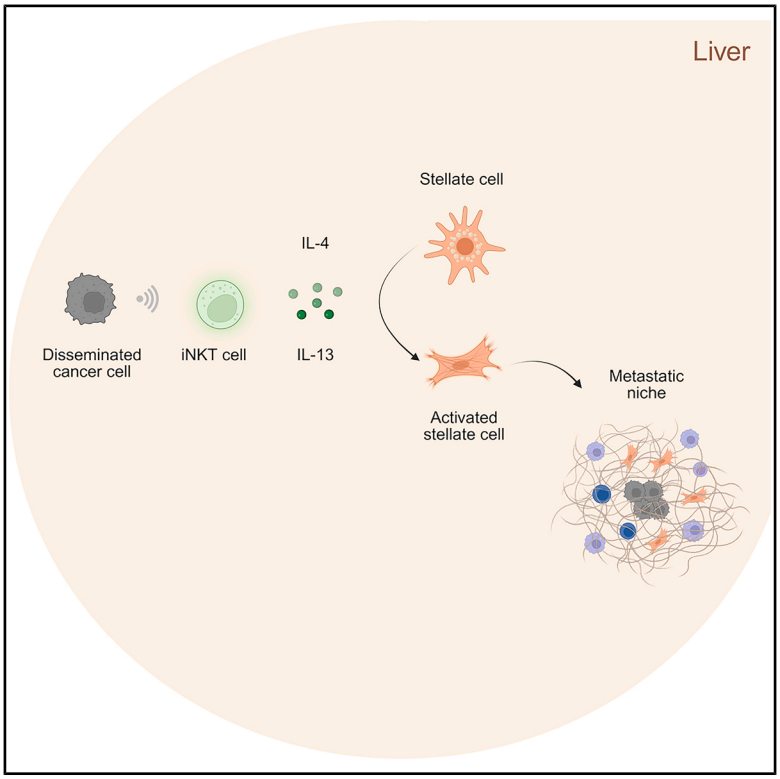

Highlights

- Hepatic iNKT cells promote metastatic outgrowth in the liver
- Hepatic iNKT cells respond to disseminated cancer cells by producing IL-4 and IL-13
- Hepatic stellate cells respond to IL-4 and IL-13 by creating a fibrotic niche
- Hepatic stellate cell-specific deletion of IL-4Rα compromises metastatic outgrowth

Authors

Marc Nater, Michael Brügger, Virginia Cecconi, ..., Christoph Schneider, Tomas Valenta, Maries van den Broek

Correspondence

maries.vandenbroek@uzh.ch

In brief

Microenvironment; Natural sciences; Biological sciences; Immunology; Immune response

Nater et al., 2025, iScience *28*, 112364
May 16, 2025
https://doi.org/10.1016/j.isci.2025.112364

CellPress

iScience

CellPress
OPEN ACCESS

Article

Hepatic iNKT cells facilitate colorectal cancer metastasis by inducing a fibrotic niche in the liver

Marc Nater,[1] Michael Brügger,[2] Virginia Cecconi,[1] Paulo Pereira,[1] Geo Forni,[1] Hakan Köksal,[1] Despoina Dimakou,[1] Michael Herbst,[1] Anna Laura Calvanese,[1] Giulia Lucchiari,[1] Christoph Schneider,[3] Tomas Valenta,[2] and Maries van den Broek[1,4,*]

[1]Institute of Experimental Immunology, University of Zurich, Zurich, Switzerland
[2]Department of Molecular Life Sciences, University of Zurich, Zurich, Switzerland
[3]Institute of Physiology, University of Zurich, Zurich, Switzerland
[4]Lead contact
*Correspondence: maries.vandenbroek@uzh.ch
https://doi.org/10.1016/j.isci.2025.112364

SUMMARY

The liver is an important metastatic organ that contains many innate immune cells, yet little is known about their role in anti-metastatic defense. We investigated how invariant natural killer T (iNKT) cells influence colorectal cancer-derived liver metastasis using different models in immunocompetent mice. We found that hepatic iNKT cells promote metastasis by creating a supportive niche for disseminated cancer cells. Mechanistically, iNKT cells respond to disseminating cancer cells by producing the fibrogenic cytokines interleukin-4 (IL-4) and IL-13 in a T cell receptor-independent manner. Selective abrogation of IL-4 and IL-13 sensing in hepatic stellate cells prevented their transdifferentiation into extracellular matrix-producing myofibroblasts, which hindered metastatic outgrowth of disseminated cancer cells. This study highlights a novel tumor-promoting axis driven by iNKT cells in the initial stages of metastasis.

INTRODUCTION

Colorectal cancer (CRC) is the third most common cancer worldwide. The liver is a frequent site of metastasis due to its direct connection with the gut, its low blood flow, and unique vascular structure.[1–3] In fact, liver metastases are found in 30–50% of CRC patients, often already at the time of diagnosis.[4,5]

A study of nearly 1,000 CRC patients identified liver fibrosis as a prognostic parameter for liver metastases.[6,7] Fibrosis is a result of protracted inflammation and is characterized by excessive extracellular matrix (ECM) deposition.[8] Functionally, fibrosis is thought to support malignant progression by fostering a growth-permissive environment for disseminated cancer cells.[9] Hepatic stellate cells (HSCs) are central mediators of the fibrotic response. Upon activation, HSCs transdifferentiate into fibrogenic myofibroblasts that drive ECM accumulation and tissue remodeling.[10,11] HSCs can be activated by a plethora of stimuli, including oxidative stress, metabolic alterations, and inflammatory cytokines, such as transforming growth factor β (TGF-β), IL-4, and IL-13.[12]

The liver is an important immune organ that constantly faces toxins from intestinal bacteria and circulating antigens. Therefore, various mechanisms that suppress adaptive immunity are in place to maintain homeostasis.[13] The liver contains an abundant population of resident innate immune cells, including natural killer (NK) cells, innate lymphocytes (ILCs), and natural killer T (NKT) cells. The latter recognize glycolipid antigens presented by the major histocompatibility complex (MHC) class I-like CD1d molecule.[14] CD1d-restricted NKT cells comprise two main subsets: type I and type II NKT cells. In mice, type I NKT cells express the invariant T cell receptor (TCR) α chain Vα14-Jα18 and are therefore referred to as invariant NKT (iNKT) cells. Experimentally, iNKT cells are usually activated by α-galactosylceramide (α-GalCer), a product of marine sponges,[15] whereas the physiological lipid antigens may be manifold and are less characterized.[14] Type II NKT cells express a polyclonal TCR repertoire and recognize self and microbial lipids.[16] In the mouse liver, 30% of all lymphocytes are NKT cells, most of which are iNKT cells.[17] Mucosal-associated invariant T (MAIT) cells are thought to be the iNKT counterpart in the human liver.[18] NKT cells patrol liver sinusoids and respond to various stimuli including TCR engagement, cytokines, and ligation of activating receptors such as Toll-like receptors (TLRs) or NKG2D.[19,20] Because of their ability to produce pro- and anti-inflammatory cytokines, studies describing the influence of NKT cells on various liver pathologies reported conflicting conclusions.[21,22] That NKT cells promote liver fibrosis, however, became unequivocally clear from different models of acute and chronic liver damage.[23–26] Although fibrosis is associated with metastasis in human cancer and the fibrogenic capacity of iNKT cells is recognized, a direct link between these processes has not yet been shown.

Here, we sought to investigate whether and how hepatic iNKT cells influence the development of liver metastasis. Using iNKT cell-deficient mouse strains and two different models for CRC-derived liver metastasis, we discovered that iNKT cells facilitate the expansion of disseminated cancer cells in the liver. Mechanistically, disseminated cancer cells stimulate iNKT cells to produce IL-4 and IL-13, which in turn activate HSCs. This results in the formation of a fibrotic niche in the liver allowing the outgrowth of disseminated cancer cells.

RESULTS

iNKT cells promote colorectal cancer-derived liver metastasis

We established two different models based on CRC organoids. The organoids (termed APTKA[27–29]) harbor deletions of the genes *Apc*, *Tp53*, and *Tgfbr2*, the activating mutation $Kras^{G12D}$, and a myristoylated version of human *AKT*. The first model (Figure S1A) involves the orthotopic injection of cancer organoids into syngeneic C57BL/6 mice using an endoscopy-guided injection method.[30,31]

The orthotopic model reflects the natural course of colorectal cancer-derived liver metastasis: a primary colon tumor develops and sheds disseminating cancer cells, which continuously seed the liver. The advantage of this model is the involvement of all steps of the metastatic cascade. The unclear and unsynchronized start of cancer cell dissemination to the liver, however, precludes the analysis of early events that occur after seeding.

To investigate the effects of cancer cell dissemination to the liver, we used the intrasplenic injection model. This procedure (Figure S1B) introduces a single bolus of cancer organoids in the spleen, which immediately enter the liver via the portal vein in a synchronized fashion. An additional advantage of this model is that we can uncouple the processes in the liver from the influence of the primary tumor. Each of these complementary models was used to address specific questions.

To study the influence of NKT cells on metastatic liver disease, we orthotopically injected APTKA organoids into *Cd1d* $^{-/-}$ *and Traj18* $^{-/-}$ mice and used C57BL/6 mice as control. *Cd1d* $^{-/-}$ mice lack both type I and II NKT cells, whereas *Traj18* $^{-/-}$ mice only lack iNKT (type I NKT) cells (Figures S1C and S1D).[32,33] We collected and analyzed primary colon tumors and livers 42 days after injection (Figure 1A). While the weight of the primary colon tumor was similar in all strains, the metastatic rate and burden were significantly lower in iNKT cell-deficient mice (Figures 1B, 1C, and S1E), indicating a tumor-promoting function for hepatic iNKT cells. *Rag1* $^{-/-}$ mice, which lack NKT, T, and B cells, showed similar protection against liver metastasis (Figures S1F–S1I), suggesting that iNKT cells do not promote metastasis through the regulation of anti-metastatic functions of adaptive immune cells.

To exclude systemic effects of the primary tumor, we intrasplenically injected luciferase-expressing APTKA organoids (APTKA-luc) into *Cd1d* $^{-/-}$, *Traj18* $^{-/-}$, and C57BL/6 mice and measured the metastatic load *ex vivo* by bioluminescence 20 days later (Figure 1D). This experimental setup confirmed the results of the orthotopic model (Figures 1E, 1F, S2A, and S2B), indicating that hepatic iNKT cells promote liver metastasis *in situ* and independently of the primary tumor. To exclude that our findings are a peculiarity of APTKA organoids, we intrasplenically injected luciferase-expressing MC38 colorectal (MC38-luc) cancer cells (Figure S2C) and obtained similar results (Figures S2D–S2F). Together, these results indicate that iNKT cells promote liver metastasis derived from colon cancer.

Cancer-cell-induced hepatic fibrosis depends on iNKT cells

Fibrosis is characterized by ECM deposition and remodeling.[8] In the liver, fibrosis is associated with the progression of liver cancer,[34] the formation of the metastatic niche,[35,36] and relies on the activation of hepatic stellate cells into collagen-producing, α-SMA^{+} myofibroblasts.[11] Using different models for liver damage, unconventional T cells were shown to be important mediators of fibrogenesis.[23–26,37–39] Histological analysis of livers in the orthotopic model (Figure 2A) showed increased fibrosis in metastatic lesions reflected by prominent collagen deposition (Figure 2B) and the abundance of α-SMA^{+} myofibroblasts (Figure 2C). In isolated metastatic nodules, we found an increased expression of *Acta2* (encoding α-SMA) and *Col1a1* (encoding type I collagen); the expression of these transcripts is associated with the activation of hepatic stellate cells (Figures 2D and 2E) and is commonly used as an indicator of fibrogenesis.[40–42] Using *Ncr1* ^{Tdtomato} *Cxcr6* ^{Gfp} reporter mice, we saw an accumulation of NKT cells (defined as CXCR6^{+} NKp46^{-} CD8^{-} cells) in established metastatic lesions (Figures 2F, S3A, and S3B). Further, we observed the colocalization of disseminated cancer cells and CXCR6^{+} cells as early as 24 h after seeding (Figure S3C), suggesting early interactions between these cell types.

To test the hypothesis that iNKT cells are responsible for the induction of a fibrotic niche, we assessed HSC activation at the time of cancer cell dissemination to the liver. Thus, we injected C57BL/6 and iNKT-deficient *Cd1d* $^{-/-}$ and *Traj18* $^{-/-}$ mice with APTKA-mCherry organoids intrasplenically to synchronize cancer cell seeding of the liver (Figure 2G). Twenty-four hours later, we saw the upregulation of *Acta2* and *Col1a1* transcripts and the deposition of collagen only in the presence of iNKT cells (Figures 2H–2K). This indicates that HSC activation by disseminated cancer cells depends on the presence of iNKT cells. The absence of iNKT cells may change the structure of the liver or influence the entry of cancer cells into the liver parenchyma, both of which could be confounding factors precluding the interpretation of the abovementioned results. We measured the seeding 3 h after intrasplenic injection of APTKA-luc cells and confirmed that the absence of iNKT cells did not affect the early seeding of cancer cells to the liver (Figures S4A–S4D). Also, APTKA-mCherry cells were detected by immunofluorescence and measured at similar amounts by quantitative reverse transcription PCR (RT-qPCR) in C57BL/6 and *Cd1d* $^{-/-}$ mice 24 h after intrasplenic injection (Figures S4E and S4F). Further, we excluded gross structural differences between C57BL/6 and *Cd1d* $^{-/-}$ mice by H&E staining of liver tissue from naive mice (Figure S4G). Taken together, our results suggest that the arrival of disseminating cancer cells in the liver activates HSCs in an iNKT-dependent manner.

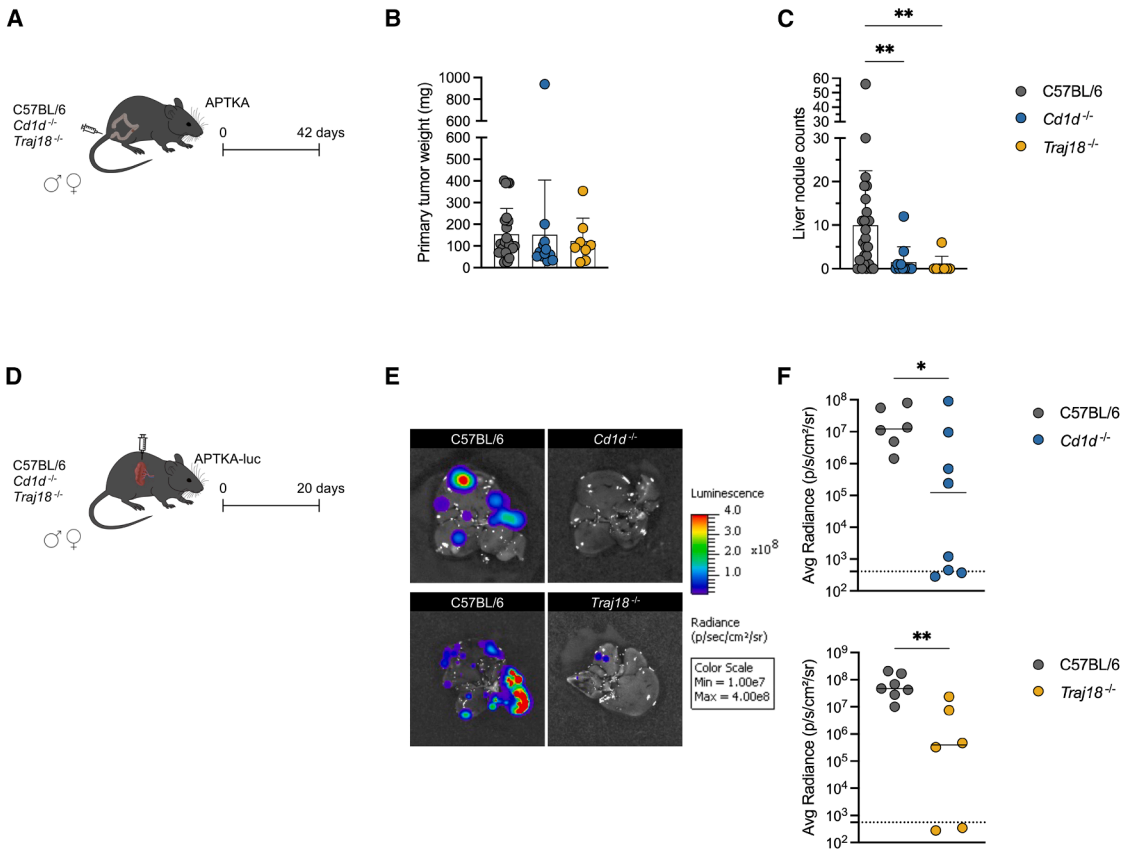

Figure 1. iNKT cells promote colorectal cancer-derived liver metastasis

(A) APTKA organoids were orthotopically injected into male and female C57BL/6, *Cd1d* $^{-/-}$, and *Traj18* $^{-/-}$ mice. Primary tumors and livers were collected and analyzed 42 days later.

(B) Weight of primary colon tumor.

(C) Quantification of liver metastasis. Pooled data from 3 experiments are shown in (B) and (C). Bars represent means ± SD. Symbols represent values from individual mice. $^{**}p < 0.01$ (one-way ANOVA).

(D) APTKA-luc organoids were intrasplenically injected into male and female C57BL/6, *Cd1d* $^{-/-}$, and *Traj18* $^{-/-}$ mice. *Ex vivo* bioluminescence of the liver was measured 20 days later.

(E) Representative measurement of liver bioluminescence and (F) quantification of liver bioluminescence. The dotted lines represent the limit of detection. The solid lines represent the median. Symbols represent values from individual mice. $^{*}p < 0.05$, $^{**}p < 0.01$ (unpaired Mann-Whitney U test).

Cancer cell dissemination induces activation of hepatic iNKT cells

iNKT cells can be activated via their TCR involving antigens presented by the non-polymorphic MHC class I-like molecule CD1d. Alternatively and like NK cells, iNKT cells can be activated by innate signals including IL-12 and ligands for TLRs or NKG2D.[20] To discriminate between TCR-dependent and independent activation, we orthotopically injected APTKA organoids in C57BL/6 mice together with a CD1d-blocking antibody or PBS (Figure S5A). CD1d-blockade did not influence the weight of the primary colon tumor or liver metastasis, suggesting that the metastasis-promoting activity of iNKT cells does not require cognate TCR interaction (Figures S5B–S5D).

To better understand how hepatic iNKT cells are activated shortly after seeding of cancer cells, we performed single-cell RNA sequencing of NKT cells sorted from livers 24 h after intrasplenic injection of PBS or APTKA organoids (Figures 3A and S6A). At steady state, most hepatic NKT cells express *Tbx21* suggesting a Th1-like polarization. This is in line with their potential to produce IL-4 and interferon gamma (IFN-γ) after TCR engagement.[17] A small proportion of NKT cells expressed Th17 signature genes such as *Rorc*, *Blk*, *Tmem176a*, *Il22*, and *Ccr6* (Figures S6B and S6C). To evaluate differences in the global population of NKT cells between naive and early metastatic livers, we performed gene set enrichment (GSE) analysis using the UCell algorithm for single-cell signature scoring.[43,44] NKT cells isolated from metastatic livers had a higher enrichment score for gene modules associated with NK cell activation (Figure S6D), underscoring our findings described above.

Graph-based clustering analysis using the Louvain algorithm[45] identified nine distinct NKT cell clusters in the liver of which cluster 4 was uniquely enriched in the early metastatic environment (Figures 3B and 3C). Cluster 4 was characterized by gene signatures associated with IFN-I response, a hallmark

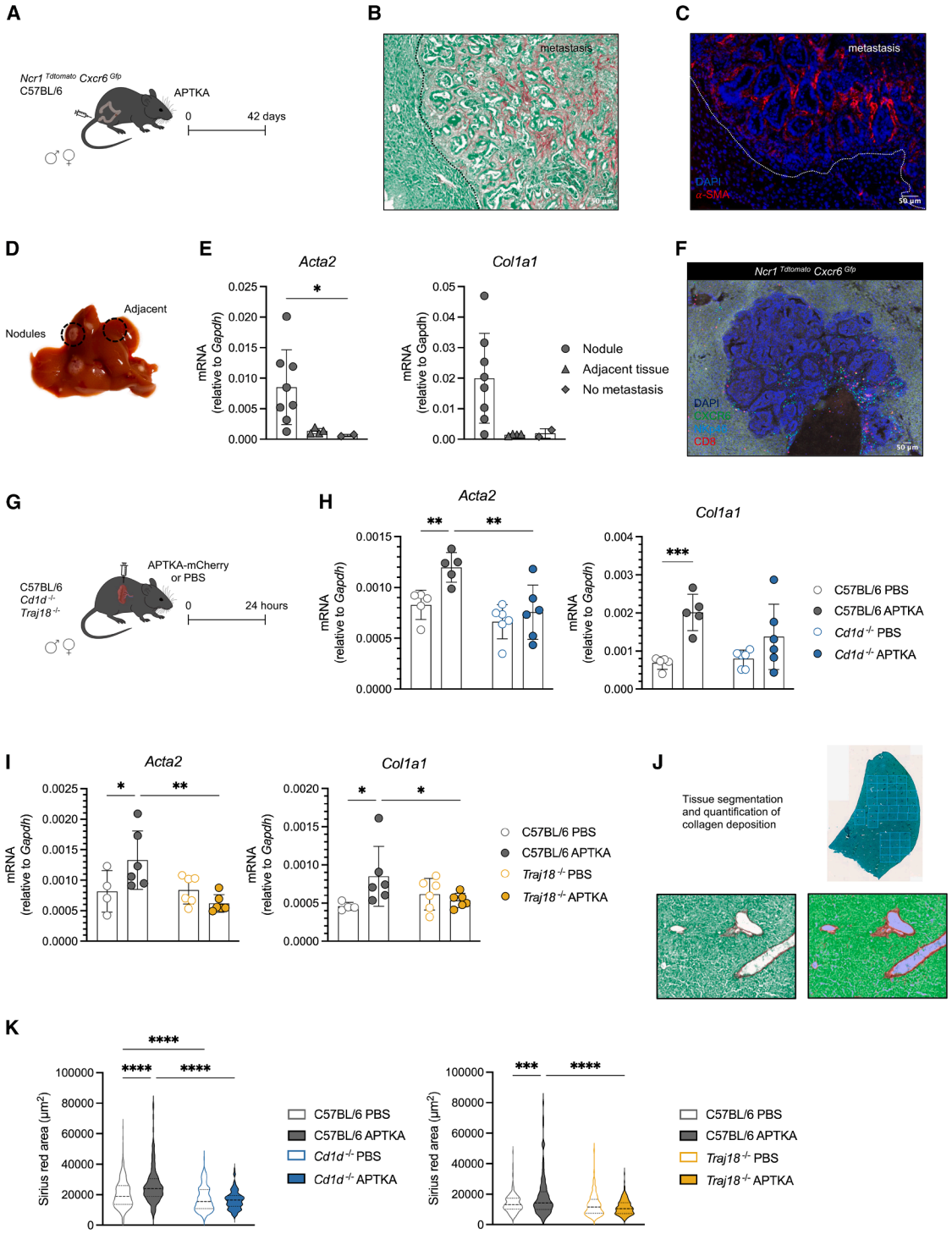

Figure 2. Cancer-cell-induced hepatic fibrosis depends on iNKT cells

(A) APTKA organoids were orthotopically injected into male and female C57BL/6 or *Ncr1* ^{Tdtomato} *Cxcr6* ^{Gfp} mice. Livers were collected and analyzed 42 days later.

(B) Representative metastatic lesion in a C57BL/6 mouse stained with Sirius red. Scale bar represents 50 µm.

(C) Representative metastatic lesion in a C57BL/6 mouse stained with DAPI and anti-α-SMA. Scale bar represents 50 µm.

(D) Parts of the metastatic livers were isolated for qRT-PCR analysis.

(E) Relative quantification of *Acta2* and *Col1a1* transcripts. Bars represent means ± SD. Symbols represent values from individual isolated liver parts. *$p < 0.05$ (one-way ANOVA).

(legend continued on next page)

of innate immune activation. The latter fits with the elevated abundance of *Ifnb1* in the liver lysate of APTKA-injected mice (Figure S6E). In addition, this cluster displayed gene signatures pointing to increased production of type 2 cytokines including IL-4, IL-5, and IL-13 (Figures 3D–3F). Overall, we showed that hepatic iNKT cells are rapidly activated by disseminated cancer cells to secrete type 2 cytokines independently of TCR signaling.

Hepatic iNKT cells respond to disseminated cancer cells by producing IL-4 and IL-13

iNKT cells can produce various cytokines upon activation, including IFN-γ, IL-4, IL-13, and TGF-β.[39] While IFN-γ has antifibrotic potential by inducing HSC apoptosis and cell-cycle arrest,[46–48] IL-4, IL-13, and TGF-β activate HSCs *in vitro* and *in vivo*.[12] We evaluated the production of these four cytokines in NKT cells following the early dissemination of cancer cells to the liver. We isolated RNA from NKT cells, which were sorted from the liver 24 h after the intrasplenic injection of APTKA-mCherry organoids or PBS (Figure 4A). Compared to NKT cells isolated from control livers, NKT cells from early metastatic livers expressed more *Il4* and *Il13* but not *Ifng* or *Tgfb1* transcripts (Figure 4B). Using *Il4* ^{4Get} reporter mice, we observed an increased number of IL-4^{+} liver iNKT cells after cancer cell dissemination, thus confirming the transcript data (Figures 4C–4E and S7A). Next, we looked for signals that can stimulate iNKT cells independently of their TCR and found a higher expression of the NKG2D ligands *H60* and *Mult1*[49] in livers from APTKA-injected than from PBS-injected mice (Figure S7B). Along the same lines, NKG2D ligand-mediated activation of unconventional T cells has been recently described as a mechanism contributing to metabolic dysfunction-associated steatohepatitis (MASH) and fibrosis.[38,50,51]

To test whether NKG2D ligation drives iNKT cell activation following cancer cell dissemination to the liver, we administered anti-NKG2D blocking antibody to *Il4* ^{4Get} reporter mice before intrasplenic injection of APTKA-organoids. Twenty-four hours later, we measured IL-4 production by iNKT cells. NKG2D blockade did not alter IL-4 production, suggesting that NKG2D engagement is not essential for early iNKT cell activation in this model (Figures S7C–S7E). Together, these results indicate that hepatic iNKT cells respond to the arrival of disseminating cancer cells with increased production of the fibrogenic cytokines IL-4 and IL-13.

Disruption of IL-4Rα signaling in hepatic stellate cells impairs fibrogenesis and diminishes metastatic growth in the liver

To investigate whether IL-4 and IL-13 directly activate HSC during the early phase of metastasis, we used *Lrat* ^{Cre} *Il4ra* ^{fl} mice that have an HSC-specific knockout of the IL-4Rα, which is the common subunit of the IL-4 and IL-13 receptors.[52,53] Following intrasplenic injection of APTKA-mCherry organoids or PBS, we observed impaired HSC activation and collagen deposition in mice with HSC-selective deficiency of IL-4Rα (Figures 5A–5D). These data indicate that iNKT-derived IL-4 and IL-13 must be sensed by HSCs for their activation and subsequent initiation of fibrosis. Consequently, we expected that compromised HSC activation and diminished fibrosis result in decreased liver metastasis. To test this hypothesis, we orthotopically injected APTKA organoids in *Lrat* ^{Cre} *Il4ra* ^{fl} mice and control littermates. Five weeks later, we assessed the development of the primary tumor and liver metastasis (Figure 5E). While the weight of the primary colon tumor was unaffected by HSC-specific deficiency of IL-4Rα, the incidence of liver metastasis was significantly reduced (Figures 5F–5H and S8A). We then investigated the individual roles of IL-4 and IL-13 in disseminated cancer cell-induced fibrogenesis. We blocked IL-4, IL-13, or both with antibodies before intrasplenic injection of APTKA-mCherry organoids or PBS and quantified the fibrogenic response. Control mice received isotype control antibodies (Figure S8B). While blockade of IL-4 or IL-13 alone did not diminish the fibrogenic response to disseminated cancer cells, simultaneous blockade of both cytokines significantly reduced collagen deposition (Figure S8C). In agreement with this finding, simultaneous blockade of both Th2 cytokines led to reduced *Col1a1* expression (Figure S8D) in the liver. Thus, IL-4 and IL-13 cooperatively drive fibrosis in response to disseminated cancer cells. Together, these results indicate that iNKT cell-derived IL-4 and IL-13 must be sensed by HSC to prepare a fibrotic niche that promotes metastatic outgrowth of disseminated cancer cells in the liver.

DISCUSSION

NKT cells are tissue-resident innate immune cells that patrol the liver sinusoids; as such, they are ideally positioned to act as immediate responders to disseminated cancer cells. The role of NKT cells in cancer is controversial. Some studies have shown tumor-restricting effects of α-GalCer-activated NKT cells in models of experimental metastasis[54–57] and in genetic models of solid tumors.[58] Along the same lines, iNKT cell-deficient mice were more susceptible to methylcholanthrene-induced fibrosarcoma. Together, these observations suggest that iNKT cells restrict cancer, even in the absence of exogenous stimulation.[59] In contrast, recent work has reported tumor-promoting functions of NKT cells in primary liver cancer and metastasis.[60–64] Those conflicting findings may be attributed to several

(F) Representative immunofluorescence image of a liver metastatic lesion in an *Ncr1* ^{Tdtomato} *Cxcr6* ^{Gfp} mouse stained with DAPI, anti-GFP, and anti-CD8. Scale bar represents 50 μm.
(G) APTKA-mCherry organoids or PBS were intrasplenically injected into male and female C57BL/6, *Cd1d* $^{-/-}$, and *Traj18* $^{-/-}$. Livers were collected and analyzed 24 h later.
(H) Relative quantification of *Acta2* and *Col1a1* transcripts in C57BL/6 and *Cd1d* $^{-/-}$ mice.
(I) Relative quantification of *Acta2* and *Col1a1* transcripts in C57BL/6 and *Traj18* $^{-/-}$ mice. Bars represent means ± SD. Symbols represent values from individual mice. *$p < 0.05$, **$p < 0.01$, ***$p < 0.001$ (two-way ANOVA).
(J) Sirius red-stained section of liver and tissue segmentation of Sirius red-positive area.
(K) Quantification of Sirius red-positive area. ***$p < 0.001$, ****$p < 0.0001$ (two-way ANOVA).

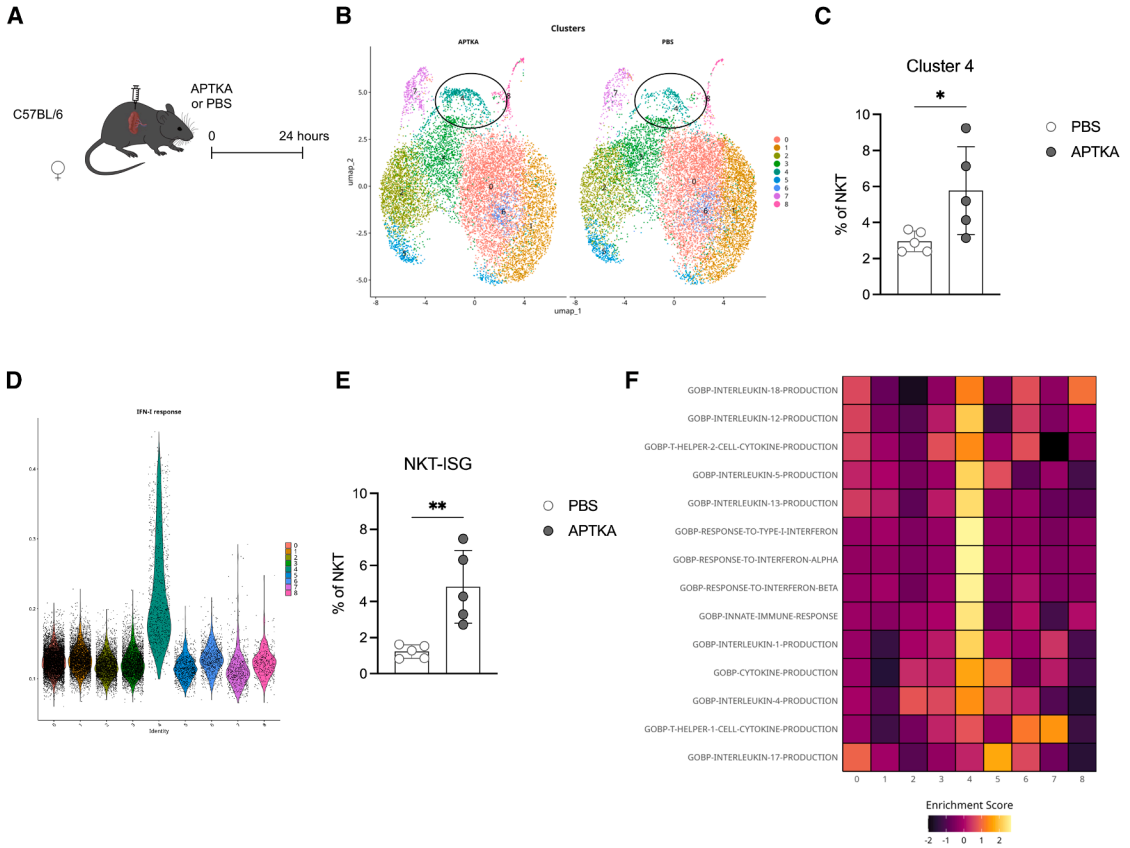

Figure 3. Cancer cell dissemination induces activation of hepatic iNKT cells

(A) APTKA organoids or PBS were intrasplenically injected into female C57BL/6 mice. Liver NKT cells (single, live, CD45$^+$, lin$^-$, CXCR6$^+$, CD8$^-$, NK1.1$^+$, NKp46$^-$ cells) were sorted 24 h later and processed following the BD Rhapsody single-cell analysis system workflow. Sequencing was performed using the NovaSeq X Plus platform. Lin = Ly6G, CD19, CD115, and F4/80.

(B) Uniform Manifold Approximation and Projection (UMAP) projection with Seurat clusters overlay.

(C) Comparison of cluster 4 frequency between PBS and APTKA-injected mice.

(D) Single-cell enrichment score of IFN-I response signature from UCell across identified clusters.

(E) Percentage of cells with an enrichment value higher than 0.19. Bars represent means ± SD. Symbols represent values from individual mice. *$p < 0.05$, **$p < 0.01$ (unpaired Mann-Whitney U test).

(F) z-transformed enrichment score of selected gene sets across identified NKT cell clusters.

factors. First, in many studies that showed a tumor-restricting function of NKT cells, NKT cells were stimulated with α-GalCer. Because α-GalCer binds with high affinity to CD1d and is a strong TCR agonist for iNKT cells, it has been used as a prototype stimulus for iNKT cells that triggers IFN-γ secretion. By using α-GalCer, the response of iNKT cells is skewed toward IFN-γ production and thus underestimates the effects of iNKT cells through the production of type 2 cytokines, hedgehog ligands, or osteopontin.[25,65] We found that hepatic iNKT cells, upon sensing disseminated cancer cells, did not produce IFN-γ but rather the fibrogenic cytokines IL-4 and IL-13. This suggests that using a strong stimulus such as α-GalCer to study the role of iNKT cells in liver metastasis may confound the results. Second, early work on iNKT cells used the first generation of the *Traj18* $^{-/-}$ strain, which was later shown to have an impaired T cell repertoire.[66] This limitation was addressed in subsequent generations of the strain, which were developed to eliminate the confounding factors present in the initial version.[67–69] Therefore, data collected using the first generation of *Traj18* $^{-/-}$ mice to study the role of iNKT cells should be cautiously interpreted. Later studies, including ours, used the second generation of *Traj18* $^{-/-}$ strains. Third, the tissue context and environmental cues influence the function of NKT cells. For instance, it was shown that microbial exposure dictates whether NKT cells are pathogenic or protective in conditions such as ulcerative colitis or liver cancer.[70,71]

A recent study has shown that tissue-resident iNKT17 cells facilitate cancer cell extravasation into the liver via IL-22.[72] Whether this mechanism is generally operative in liver metastasis is currently unknown. Also, due to the unavailability of tools that target iNKT or NKT cells, mechanistic studies on how these cells influence liver metastasis are largely lacking.

We investigated whether and how iNKT cells influence the development of hepatic metastasis using two mechanistically different models for CRC-derived liver metastasis and two mouse strains that lacked either all NKT cells (*Cd1d* $^{-/-}$) or

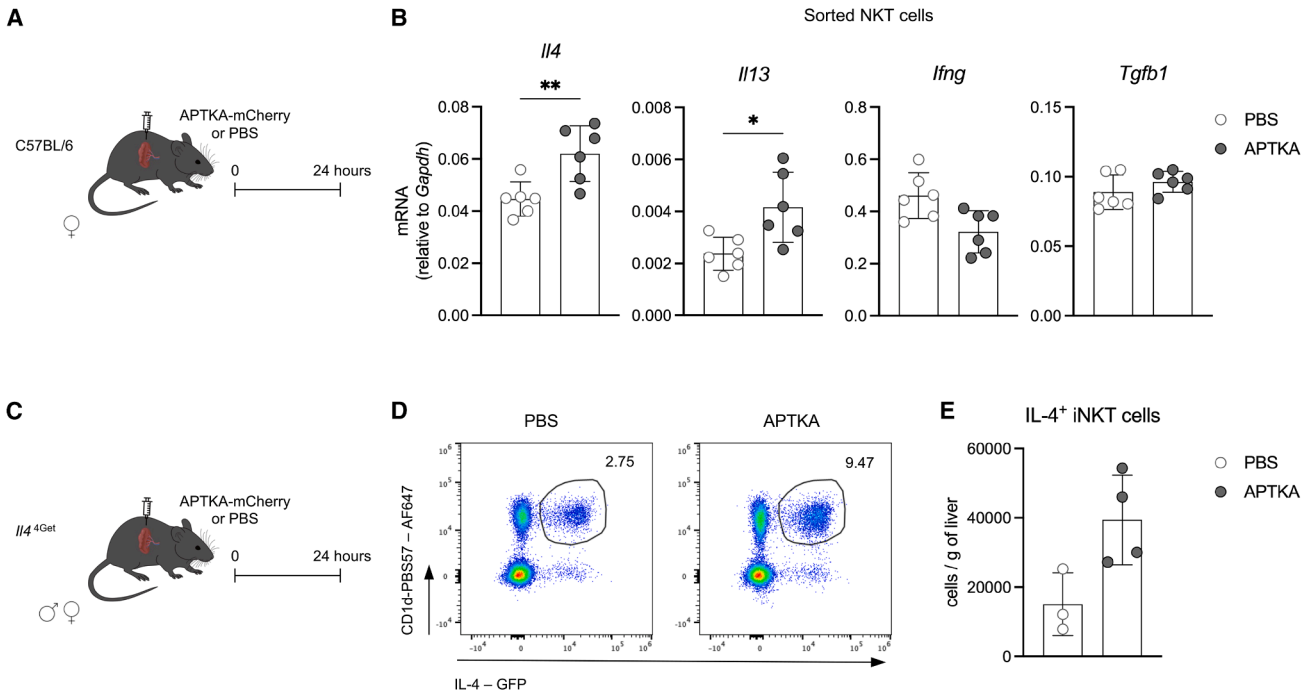

Figure 4. Hepatic iNKT cells respond to disseminated cancer cells by producing IL-4 and IL-13

(A) APTKA-mCherry organoids or PBS were intrasplenically injected into female C57BL/6 mice. NKT cells (single, live, CD45$^+$, lin$^-$, CXCR6$^+$, CD8$^-$, NK1.1$^+$, NKp46$^-$ cells) were sorted from livers 24 h later and processed for mRNA isolation. Lin = Ly6G, CD19, CD115, and F4/80.

(B) Relative quantification of *Il4*, *Il13*, *Ifng*, and *Tgfb1* transcripts.

(C) APTKA-mCherry organoids or PBS were intrasplenically injected into male and female *Il4* $^{4Get/wt}$ mice. Livers were collected 24 h later and processed for flow cytometry.

(D) Representative dot plots and (E) quantification of IL-4$^+$ iNKT cells in the liver of PBS- and APTKA-injected mice. Samples were pre-gated on single, live, CD45$^+$, Ly6G$^-$, CD19$^-$, TCR-β$^+$, CD11b$^-$ cells. Bars represent means ± SD. Symbols represent values from individual mice. *$p < 0.05$, **$p < 0.01$ (unpaired Mann-Whitney U test).

only iNKT cells (*Traj18* $^{-/-}$). We found that in the absence of iNKT cells, disseminated cancer cells failed to form progressive metastatic lesions despite equal seeding of the liver. Thus, iNKT cells promote the survival and/or proliferation of disseminated cancer cells, which are important bottlenecks for the establishment of liver metastasis. These findings prompted the hypothesis that arriving cancer cells are sensed by iNKT cells leading to their activation. To test this hypothesis, we characterized iNKT cells isolated from early metastatic and naive livers by single-cell RNA sequencing. Besides some generic signatures of innate activation, we found that hepatic iNKT cells displayed an increased expression of IL-4 and IL-13 within a day after sensing disseminated cancer cells. These two type 2 cytokines raised our interest because of their established role in liver fibrosis.[73] We show that IL-4 and IL-13 directly activate HSCs, leading to their transdifferentiation into myofibroblasts and subsequent deposition of extracellular matrix. HSCs were recently identified as the primary source of myofibroblasts in the liver and as key players in fibrosis.[11] Depletion of HSCs showed their essential role in metastatic outgrowth in the liver.[74] The underlying mechanisms, however, were not addressed in this study and remain largely unexplored. We discovered here that HSC-specific ablation of the IL-4Rα, which binds both IL-4 and IL-13, significantly impaired fibrosis and reduced the metastatic burden, underscoring the crucial role of the IL-4Rα signaling pathway in the establishment of the metastatic niche. Our findings are in line with studies aiming to identify fibrotic drivers in type 2-driven disease. Indeed, *Il4ra* $^{-/-}$ mice were protected against IL-33-driven fibrosis.[75] Further, ablating IL-4Rα signaling in PDGFRB$^+$ fibroblasts but not in albumin-expressing hepatocytes or cholangiocytes protected mice from liver fibrosis driven by IL-13 overexpression or *Schistosoma mansoni* infection.[76] While we showed that HSCs undergo functional changes in response to IL-4 and IL-13, we did not formally exclude the possibility that other cell types produce type 2 cytokines. The fact that the HSC-specific *Il4ra* knockout phenocopies the results in iNKT cell-deficient mice, however, strongly suggests that iNKT cells are a key source of IL-4 and IL-13 driving HSC activation in our model. In conclusion, by establishing the mechanistic link between iNKT cells, fibrosis, and liver metastasis, we discovered an IL-4/IL-13-driven tumor-promoting function of iNKT cells in the early stages of liver metastasis.

Limitations of the study

We investigated the role of hepatic iNKT cells in metastasis from colorectal cancer. Using two experimental models and two cell lines, we identified an axis involving iNKT cells and hepatic stellate cells that facilitates metastasis in its early stages. This

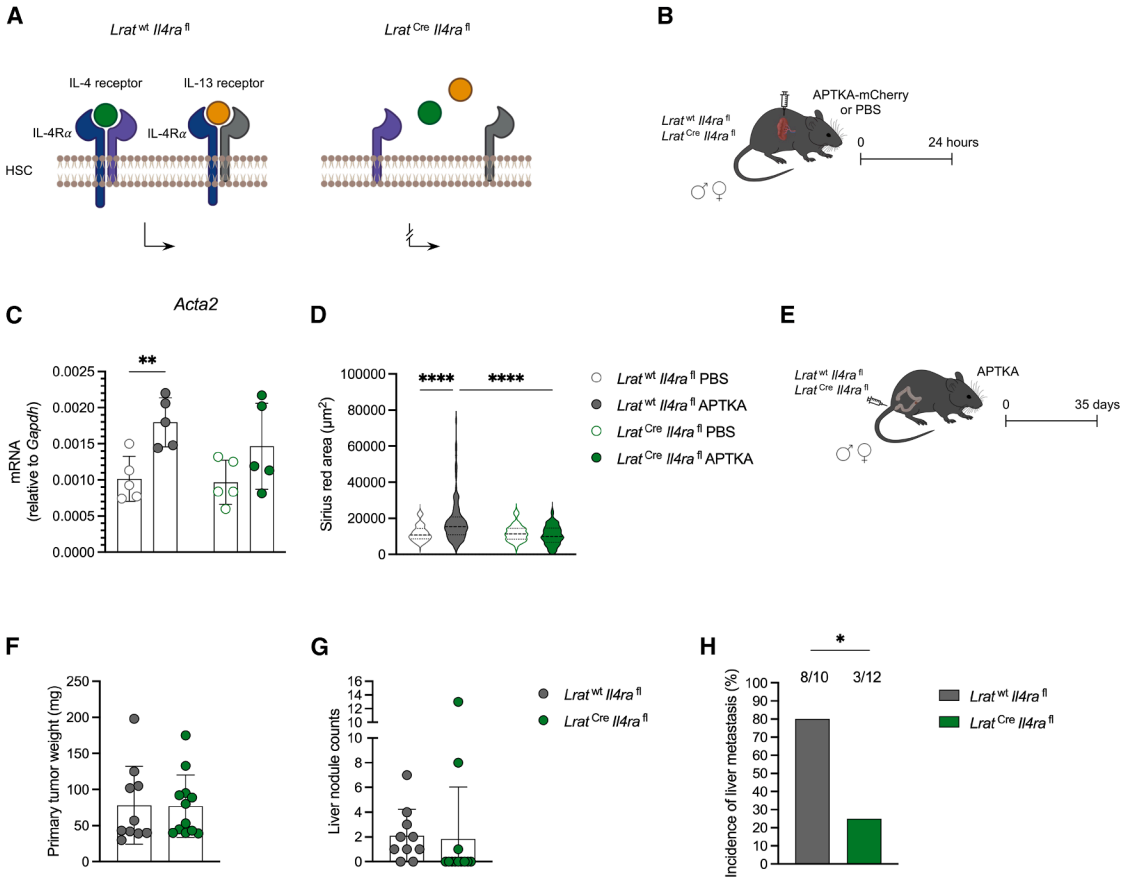

Figure 5. Disruption of IL-4Rα signaling in hepatic stellate cells impairs fibrogenesis and diminishes metastatic growth in the liver

(A) Scheme explaining the genetic model used.

(B) APTKA-mCherry organoids were intrasplenically injected into male and female *Lrat* $^{Cre/wt}$ *Il4ra* $^{fl/fl}$ and *Lrat* $^{wt/wt}$ *Il4ra* $^{fl/fl}$ mice. Livers were collected 24 h later.

(C) Relative quantification of *Acta2* transcript.

(D) Quantification of Sirius red-positive area. Bars represent means ± SD. Symbols represent values from individual mice. $^{**}p < 0.01$, $^{****}p < 0.0001$ (two-way ANOVA).

(E) APTKA organoids were orthotopically injected into male and female *Lrat* $^{Cre/wt}$ *Il4ra* $^{fl/fl}$ and *Lrat* $^{wt/wt}$ *Il4ra* $^{fl/fl}$ mice. Primary tumors and livers were collected and analyzed 35 days later.

(F) Weight of primary colon tumor.

(G) Quantification of liver metastasis. Bars represent means ± SD. Symbols represent values from individual mice (unpaired Mann-Whitney U test).

(H) Incidence of liver metastasis in tumor-bearing mice. $^{*}p < 0.05$ (Fisher's exact test).

mechanism acts shortly after cancer cells have disseminated to the liver. We found that iNKT-derived IL-4 and IL-13 are essential mediators of hepatic stellate cell activation; however, we did not uncover the mechanism by which disseminated cancer cells activate iNKT cells. Further, while our histological analyses demonstrate the liver as an important site of interaction between iNKT cells and disseminated cancer cells, we do not exclude the possibility of additional encounters at extrahepatic sites, such as the bone marrow.

Validating these findings in human samples would require liver tissue capturing the earliest stages of metastasis. However, liver biopsies are generally performed only when metastases are clinically apparent and therefore significantly advanced. Furthermore, the sparsity of disseminated cancer cells often causes them to go undetected in standard histopathological assessments of suspected lesions. Consequently, there is a lack of sufficiently large clinical cohorts of colorectal cancer patients with early liver dissemination, limiting our ability to examine the initial events of the metastatic process.

RESOURCE AVAILABILITY

Lead contact

Further information and requests for resources and reagents should be directed to and will be fulfilled by the lead contact, Maries van den Broek (maries.vandenbroek@uzh.ch).

Materials availability

The materials generated for this study can be provided upon reasonable request.

Data and code availability

- All data reported in this paper will be shared by the lead contact upon reasonable request.

- This paper does not report original code.
- The sequencing data that were generated for this study have been deposited in Gene Expression Omnibus under the accession number GSE274890.

Received: September 19, 2024
Revised: March 5, 2025
Accepted: April 2, 2025
Published: April 6, 2025

ACKNOWLEDGMENTS

This work was supported by the University Research Priority Program "Translational Cancer Research" (University of Zurich; MvdB), SKINTEGRITY.ch (University of Zurich; M.v.d.B.), the Hartmann-Müller-Foundation (M.N.), the Swiss National Science Foundation (310030_208145; M.v.d.B.), and the Swiss Cancer League (KFS-5104-08-2020; M.v.d.B.).

The authors thank Florian Greten (Georg-Speyer-Haus, Frankfurt am Main, Germany) for sharing the APTKA organoids, and Andreas Moor and Costanza Borrelli (ETH Zurich) for initial help with organoid handling. We thank the personnel of the Laboratory Animal Services Center (LASC, University of Zurich) for expert animal care. We thank Stephan Benke (Cytometry Facility, University of Zurich) for support with flow cytometry data analysis. We thank Tatiane Gorski (Cytometry Facility, University of Zurich) and Hubert Rehrauer (Functional Genomic Center Zurich) for help with scRNA-sequencing, and Achim Weber, Christian Münz, Hassan Fazilaty, and Sònia Tugues (University of Zurich), Matteo Iannacone (Ospedale San Raffaele, Milano, Italy), and Martin Guilliams (VIB Ghent, Belgium) for helpful discussion and suggestions. The graphical abstract was created in BioRender.com.

AUTHOR CONTRIBUTIONS

M.N. and M.v.d.B. conceived the experiments and wrote the manuscript; M. N., M.B., V.C., P.P., G.F., D.D., M.H., A.L.C., G.L., and T.V. performed the experiments; C.S. provided essential reagents; M.N. and H.K. analyzed the data; M.v.d.B. secured funding; all the authors reviewed the results and approved the final manuscript.

DECLARATION OF INTERESTS

The authors declare no competing interests.

STAR★METHODS

Detailed methods are provided in the online version of this paper and include the following:

- KEY RESOURCES TABLE
- EXPERIMENTAL MODEL AND STUDY PARTICIPANT DETAILS
  - Mice
  - Organoids and cancer cell lines
- METHOD DETAILS
  - Collection and expansion of APTKA organoids
  - Orthotopic injection of APTKA organoids
  - Intrasplenic injection of APTKA organoids or MC38 cells
  - *Ex vivo* bioluminescence
  - Injection of monoclonal antibodies
  - Sorting of NKT cells
  - qRT-PCR
  - Flow cytometry
  - Immunofluorescence
  - Sirius red staining
  - Single-cell RNA sequencing
- QUANTIFICATION AND STATISTICAL ANALYSIS

SUPPLEMENTAL INFORMATION

Supplemental information can be found online at https://doi.org/10.1016/j.isci.2025.112364.

REFERENCES

1. Ficht, X., and Iannacone, M. (2020). Immune surveillance of the liver by T cells. Sci. Immunol. *5*, eaba2351. https://doi.org/10.1126/sciimmunol.aba2351.
2. Kubes, P., and Jenne, C. (2018). Immune Responses in the Liver. Annu. Rev. Immunol. *36*, 247–277. https://doi.org/10.1146/annurev-immunol-051116-052415.
3. Cañellas-Socias, A., Sancho, E., and Batlle, E. (2024). Mechanisms of metastatic colorectal cancer. Nat. Rev. Gastroenterol. Hepatol. *21*, 609–625. https://doi.org/10.1038/s41575-024-00934-z.
4. Nordlinger, B., Sorbye, H., Glimelius, B., Poston, G.J., Schlag, P.M., Rougier, P., Bechstein, W.O., Primrose, J.N., Walpole, E.T., Finch-Jones, M., et al. (2008). Perioperative chemotherapy with FOLFOX4 and surgery versus surgery alone for resectable liver metastases from colorectal cancer (EORTC Intergroup trial 40983): a randomised controlled trial. Lancet *371*, 1007–1016. https://doi.org/10.1016/S0140-6736(08)60455-9.
5. Slesser, A.A.P., Simillis, C., Goldin, R., Brown, G., Mudan, S., and Tekkis, P.P. (2013). A meta-analysis comparing simultaneous versus delayed resections in patients with synchronous colorectal liver metastases. Surg. Oncol. *22*, 36–47. https://doi.org/10.1016/j.suronc.2012.11.002.
6. Hu, X., Marietta, A., Dai, W.X., Li, Y.Q., Ma, X.J., Zhang, L., Cai, S.J., and Peng, J.J. (2020). Prediction of hepatic metastasis and relapse in colorectal cancers based on concordance analyses with liver fibrosis scores. Clin. Transl. Med. *9*, 13. https://doi.org/10.1186/s40169-020-0264-3.
7. Kondo, T., Okabayashi, K., Hasegawa, H., Tsuruta, M., Shigeta, K., and Kitagawa, Y. (2016). The impact of hepatic fibrosis on the incidence of liver metastasis from colorectal cancer. Br. J. Cancer *115*, 34–39. https://doi.org/10.1038/bjc.2016.155.
8. Pellicoro, A., Ramachandran, P., Iredale, J.P., and Fallowfield, J.A. (2014). Liver fibrosis and repair: immune regulation of wound healing in a solid organ. Nat. Rev. Immunol. *14*, 181–194. https://doi.org/10.1038/nri3623.
9. Patras, L., Shaashua, L., Matei, I., and Lyden, D. (2023). Immune determinants of the pre-metastatic niche. Cancer Cell *41*, 546–572. https://doi.org/10.1016/j.ccell.2023.02.018.
10. Hammerich, L., and Tacke, F. (2023). Hepatic inflammatory responses in liver fibrosis. Nat. Rev. Gastroenterol. Hepatol. *20*, 633–646. https://doi.org/10.1038/s41575-023-00807-x.
11. Mederacke, I., Hsu, C.C., Troeger, J.S., Huebener, P., Mu, X., Dapito, D. H., Pradere, J.-P., and Schwabe, R.F. (2013). Fate tracing reveals hepatic stellate cells as dominant contributors to liver fibrosis independent of its aetiology. Nat. Commun. *4*, 2823. https://doi.org/10.1038/ncomms3823.
12. Tsuchida, T., and Friedman, S.L. (2017). Mechanisms of hepatic stellate cell activation. Nat. Rev. Gastroenterol. Hepatol. *14*, 397–411. https://doi.org/10.1038/nrgastro.2017.38.
13. Crispe, I.N. (2003). Hepatic T cells and liver tolerance. Nat. Rev. Immunol. *3*, 51–62. https://doi.org/10.1038/nri981.
14. Rossjohn, J., Pellicci, D.G., Patel, O., Gapin, L., and Godfrey, D.I. (2012). Recognition of CD1d-restricted antigens by natural killer T cells. Nat. Rev. Immunol. *12*, 845–857. https://doi.org/10.1038/nri3328.
15. Kawano, T., Cui, J., Koezuka, Y., Toura, I., Kaneko, Y., Motoki, K., Ueno, H., Nakagawa, R., Sato, H., Kondo, E., et al. (1997). CD1d-Restricted and TCR-Mediated Activation of Vα14 NKT Cells by Glycosylceramides. Science *278*, 1626–1629. https://doi.org/10.1126/science.278.5343.1626.
16. Godfrey, D.I., MacDonald, H.R., Kronenberg, M., Smyth, M.J., and Van Kaer, L. (2004). NKT cells: What's in a name? Nat. Rev. Immunol. *4*, 231–237. https://doi.org/10.1038/nri1309.

17. Crosby, C.M., and Kronenberg, M. (2018). Tissue-specific functions of invariant natural killer T cells. Nat. Rev. Immunol. *18*, 559–574. https://doi.org/10.1038/s41577-018-0034-2.

18. Pellicci, D.G., Koay, H.-F., and Berzins, S.P. (2020). Thymic development of unconventional T cells: how NKT cells, MAIT cells and γδ T cells emerge. Nat. Rev. Immunol. *20*, 756–770. https://doi.org/10.1038/s41577-020-0345-y.

19. Geissmann, F., Cameron, T.O., Sidobre, S., Manlongat, N., Kronenberg, M., Briskin, M.J., Dustin, M.L., and Littman, D.R. (2005). Intravascular immune surveillance by CXCR6+ NKT cells patrolling liver sinusoids. PLoS Biol. *3*, e113–e0661. https://doi.org/10.1371/journal.pbio.0030113.

20. Brennan, P.J., Brigl, M., and Brenner, M.B. (2013). Invariant natural killer T cells: An innate activation scheme linked to diverse effector functions. Nat. Rev. Immunol. *13*, 101–117. https://doi.org/10.1038/nri3369.

21. Yang, A.Y.-P., Wistuba-Hamprecht, K., Greten, T.F., and Ruf, B. (2024). Innate-like T cells in liver disease. Trends Immunol. *45*, 535–548. https://doi.org/10.1016/j.it.2024.05.008.

22. Gu, X., Chu, Q., Ma, X., Wang, J., Chen, C., Guan, J., Ren, Y., Wu, S., and Zhu, H. (2022). New insights into iNKT cells and their roles in liver diseases. Front. Immunol. *13*, 1035950–1036017. https://doi.org/10.3389/fimmu.2022.1035950.

23. Ishikawa, S., Ikejima, K., Yamagata, H., Aoyama, T., Kon, K., Arai, K., Takeda, K., and Watanabe, S. (2011). CD1d-restricted natural killer T cells contribute to hepatic inflammation and fibrogenesis in mice. J. Hepatol. *54*, 1195–1204. https://doi.org/10.1016/j.jhep.2010.08.022.

24. Jin, Z., Sun, R., Wei, H., Gao, X., Chen, Y., and Tian, Z. (2011). Accelerated liver fibrosis in hepatitis B virus transgenic mice: Involvement of natural killer T cells. Hepatology *53*, 219–229. https://doi.org/10.1002/hep.23983.

25. Syn, W.K., Agboola, K.M., Swiderska, M., Michelotti, G.A., Liaskou, E., Pang, H., Xie, G., Philips, G., Chan, I.S., Karaca, G.F., et al. (2012). NKT-associated hedgehog and osteopontin drive fibrogenesis in non-alcoholic fatty liver disease. Gut *61*, 1323–1329. https://doi.org/10.1136/gutjnl-2011-301857.

26. Wehr, A., Baeck, C., Heymann, F., Niemietz, P.M., Hammerich, L., Martin, C., Zimmermann, H.W., Pack, O., Gassler, N., Hittatiya, K., et al. (2013). Chemokine Receptor CXCR6-Dependent Hepatic NK T Cell Accumulation Promotes Inflammation and Liver Fibrosis. J. Immunol. *190*, 5226–5236. https://doi.org/10.4049/jimmunol.1202909.

27. Varga, J., Nicolas, A., Petrocelli, V., Pesic, M., Mahmoud, A., Michels, B. E., Etlioglu, E., Yepes, D., Häupl, B., Ziegler, P.K., et al. (2020). AKT-dependent NOTCH3 activation drives tumor progression in a model of mesenchymal colorectal cancer. J. Exp. Med. *217*, e20191515. https://doi.org/10.1084/jem.20191515.

28. Nicolas, A.M., Pesic, M., and Florian, R. (2022). Protocol Image-guided radiotherapy in an orthotopic mouse model of rectal cancer model of rectal cancer. STAR Protoc *3*, 101749. https://doi.org/10.1016/j.xpro.2022.101749.

29. Nicolas, A.M., Pesic, M., Engel, E., Ziegler, P.K., Diefenhardt, M., Kennel, K.B., Buettner, F., Conche, C., Petrocelli, V., Elwakeel, E., et al. (2022). Inflammatory fibroblasts mediate resistance to neoadjuvant therapy in rectal cancer. Cancer Cell *40*, 168–184. https://doi.org/10.1016/j.ccell.2022.01.004.

30. Roper, J., Tammela, T., Cetinbas, N.M., Akkad, A., Roghanian, A., Rickelt, S., Almeqdadi, M., Wu, K., Oberli, M.A., Sánchez-Rivera, F.J., et al. (2017). In vivo genome editing and organoid transplantation models of colorectal cancer and metastasis. Nat. Biotechnol. *35*, 569–576. https://doi.org/10.1038/nbt.3836.

31. Roper, J., Tammela, T., Akkad, A., Almeqdadi, M., Santos, S.B., Jacks, T., and Yilmaz, Ö.H. (2018). Colonoscopy-based colorectal cancer modeling in mice with CRISPR-Cas9 genome editing and organoid transplantation. Nat. Protoc. *13*, 217–234. https://doi.org/10.1038/nprot.2017.136.

32. Jahng, A., Maricic, I., Aguilera, C., Cardell, S., Halder, R.C., and Kumar, V. (2004). Prevention of Autoimmunity by Targeting a Distinct, Noninvariant CD1d-reactive T Cell Population Reactive to Sulfatide. J. Exp. Med. *199*, 947–957. https://doi.org/10.1084/jem.20031389.

33. Singh, A.K., Tripathi, P., and Cardell, S.L. (2018). Type II NKT Cells : An Elusive Population With Immunoregulatory Properties. Front. Immunol. *9*, 1969. https://doi.org/10.3389/fimmu.2018.01969.

34. Affo, S., Yu, L.X., and Schwabe, R.F. (2017). The Role of Cancer-Associated Fibroblasts and Fibrosis in Liver Cancer. Annu. Rev. Pathol. *12*, 153–186. https://doi.org/10.1146/annurev-pathol-052016-100322.

35. Costa-Silva, B., Aiello, N.M., Ocean, A.J., Singh, S., Zhang, H., Thakur, B. K., Becker, A., Hoshino, A., Mark, M.T., Molina, H., et al. (2015). Pancreatic cancer exosomes initiate pre-metastatic niche formation in the liver. Nat. Cell Biol. *17*, 816–826. https://doi.org/10.1038/ncb3169.

36. Lee, J.W., Stone, M.L., Porrett, P.M., Thomas, S.K., Komar, C.A., Li, J.H., Delman, D., Graham, K., Gladney, W.L., Hua, X., et al. (2019). Hepatocytes direct the formation of a pro-metastatic niche in the liver. Nature *567*, 249–252. https://doi.org/10.1038/s41586-019-1004-y.

37. Mabire, M., Pushpa, H., Adel, H., Wan, J., Allaire, M., Rola, A.S., Thibault-Sogorb, T., Weiss, E., Paradis, V., de la Grange, P., et al. (2023). MAIT cell inhibition promotes liver fibrosis regression by reprogramming macrophage phenotype. Nat. Commun. *14*, 1830. https://doi.org/10.1038/s41467-023-37453-5.

38. Marinović, S., Lenartić, M., Mladenić, K., Šestan, M., Kavazović, I., Benić, A., Krapić, M., Rindlisbacher, L., Cokarić Brdovčak, M., Sparano, C., et al. (2023). NKG2D-mediated detection of metabolically stressed hepatocytes by innate-like T cells is essential for initiation of NASH and fibrosis. Sci Immunol *8*, 1–19. https://doi.org/10.1126/sciimmunol.add1599.

39. Kumar, V., Hertz, M., Agro, A., and Byrne, A.J. (2023). Type 1 invariant natural killer T cells in chronic inflammation and tissue fibrosis. Front. Immunol. *14*, 1260503–1260509. https://doi.org/10.3389/fimmu.2023.1260503.

40. Affo, S., Nair, A., Brundu, F., Ravichandra, A., Bhattacharjee, S., Matsuda, M., Chin, L., Filliol, A., Wen, W., Song, X., et al. (2021). Promotion of cholangiocarcinoma growth by diverse cancer-associated fibroblast subpopulations. Cancer Cell *39*, 866–882. https://doi.org/10.1016/j.ccell.2021.03.012.

41. Filliol, A., Saito, Y., Nair, A., Dapito, D.H., Yu, L.-X., Ravichandra, A., Bhattacharjee, S., Affo, S., Fujiwara, N., Su, H., et al. (2022). Opposing roles of hepatic stellate cell subpopulations in hepatocarcinogenesis. Nature *610*, 356–365. https://doi.org/10.1038/s41586-022-05289-6.

42. Tsuchiya, Y., Seki, T., Kobayashi, K., Komazawa-Sakon, S., Shichino, S., Nishina, T., Fukuhara, K., Ikejima, K., Nagai, H., Igarashi, Y., et al. (2023). Fibroblast growth factor 18 stimulates the proliferation of hepatic stellate cells, thereby inducing liver fibrosis. Nat. Commun. *14*, 6304. https://doi.org/10.1038/s41467-023-42058-z.

43. Andreatta, M., and Carmona, S.J. (2021). UCell: Robust and scalable single-cell gene signature scoring. Comput. Struct. Biotechnol. J. *19*, 3796–3798. https://doi.org/10.1016/j.csbj.2021.06.043.

44. Borcherding, N., Vishwakarma, A., Voigt, A.P., Bellizzi, A., Kaplan, J., Nepple, K., Salem, A.K., Jenkins, R.W., Zakharia, Y., and Zhang, W. (2021). Mapping the immune environment in clear cell renal carcinoma by single-cell genomics. Commun. Biol. *4*, 122. https://doi.org/10.1038/s42003-020-01625-6.

45. Blondel, V.D., Guillaume, J.-L., Lambiotte, R., and Lefebvre, E. (2008). Fast unfolding of communities in large networks. J. Stat. Mech. *2008*, P10008. https://doi.org/10.1088/1742-5468/2008/10/P10008.

46. Jeong, W.I., Park, O., Suh, Y.G., Byun, J.S., Park, S.Y., Choi, E., Kim, J.K., Ko, H., Wang, H., Miller, A.M., and Gao, B. (2011). Suppression of innate immunity (natural killer cell/interferon-γ) in the advanced stages of liver fibrosis in mice. Hepatology *53*, 1342–1351. https://doi.org/10.1002/hep.24190.

47. Baroni, G.S., D'Ambrosio, L., Curto, P., Casini, A., Mancini, R., Jezequel, A.M., and Benedetti, A. (1996). Interferon gamma decreases hepatic stellate cell activation and extracellular matrix deposition in rat liver fibrosis.

Hepatology *23*, 1189–1199. https://doi.org/10.1053/jhep.1996.v23.pm0008621153.

48. Jeong, W.I., Park, O., and Gao, B. (2008). Abrogation of the Antifibrotic Effects of Natural Killer Cells/Interferon-γ Contributes to Alcohol Acceleration of Liver Fibrosis. Gastroenterology *134*, 248–258. https://doi.org/10.1053/j.gastro.2007.09.034.

49. Raulet, D.H. (2003). Roles of the NKG2D immunoreceptor and its ligands. Nat. Rev. Immunol. *3*, 781–790. https://doi.org/10.1038/nri1199.

50. Vilarinho, S., Ogasawara, K., Nishimura, S., Lanier, L.L., and Baron, J.L. (2007). Blockade of NKG2D on NKT cells prevents hepatitis and the acute immune response to hepatitis B virus. Proc. Natl. Acad. Sci. USA *104*, 18187–18192. https://doi.org/10.1073/pnas.0708968104.

51. Kuylenstierna, C., Björkström, N.K., Andersson, S.K., Sahlström, P., Bosnjak, L., Paquin-Proulx, D., Malmberg, K.J., Ljunggren, H.G., Moll, M., and Sandberg, J.K. (2011). NKG2D performs two functions in invariant NKT cells: Direct TCR-independent activation of NK-like cytolysis and co-stimulation of activation by CD1d. Eur. J. Immunol. *41*, 1913–1923. https://doi.org/10.1002/eji.200940278.

52. Allen, J.E. (2023). IL-4 and IL-13: Regulators and Effectors of Wound Repair. Annu. Rev. Immunol. *41*, 229–254.

53. Herbert, D.R., Hölscher, C., Mohrs, M., Arendse, B., Schwegmann, A., Radwanska, M., Leeto, M., Kirsch, R., Hall, P., Mossmann, H., et al. (2004). Alternative Macrophage Activation Is Essential for Survival during Schistosomiasis and Downmodulates T Helper 1 Responses and Immunopathology. Immunity *21*, 455. https://doi.org/10.1016/j.immuni.2004.08.004.

54. Nishikawa, H., Kato, T., Tanida, K., Hiasa, A., Tawara, I., Ikeda, H., Ikarashi, Y., Wakasugi, H., Kronenberg, M., Nakayama, T., et al. (2003). CD4 + CD25 + T cells responding to serologically defined autoantigens suppress antitumor immune responses. Proc. Natl. Acad. Sci. USA *100*, 10902–10906. https://doi.org/10.1073/pnas.1834479100.

55. Smyth, M.J., Crowe, N.Y., Pellicci, D.G., Kyparissoudis, K., Kelly, J.M., Takeda, K., Yagita, H., and Godfrey, D.I. (2002). Sequential production of interferon-γ by NK1.1+ T cells and natural killer cells is essential for the antimetastatic effect of α-galactosylceramide. Blood *99*, 1259–1266. https://doi.org/10.1182/blood.V99.4.1259.

56. Miyagi, T., Takehara, T., Tatsumi, T., Kanto, T., Suzuki, T., Jinushi, M., Sugimoto, Y., Sasaki, Y., Hori, M., and Hayashi, N. (2003). CD1d-mediated stimulation of natural killer T cells selectively activates hepatic natural killer cells to eliminate experimentally disseminated hepatoma cells in murine liver. Int. J. Cancer *106*, 81–89. https://doi.org/10.1002/ijc.11163.

57. Toura, I., Kawano, T., Akutsu, Y., Nakayama, T., Ochiai, T., and Taniguchi, M. (1999). Cutting Edge: Inhibition of Experimental Tumor Metastasis by Dendritic Cells Pulsed with α -Galactosylceramide. J. Immunol. *163*, 2387–2391.

58. Hayakawa, Y., Rovero, S., Forni, G., and Smyth, M.J. (2003). α--Galactosylceramide (KRN7000) suppression of chemical- and oncogene-dependent carcinogenesis. Proc. Natl. Acad. Sci. USA *100*, 9464–9469.

59. Crowe, N.Y., Smyth, M.J., and Godfrey, D.I. (2002). A Critical Role for Natural Killer T Cells in Immunosurveillance of Methylcholanthrene-induced Sarcomas. J. Exp. Med. *196*, 119–127. https://doi.org/10.1084/jem.20020092.

60. Yang, W., Li, H., Mayhew, E., Mellon, J., Chen, P.W., and Niederkorn, J.Y. (2011). NKT cell exacerbation of liver metastases arising from melanomas transplanted into either the eyes or spleens of mice. Investig. Ophthalmol. Vis. Sci. *52*, 3094–3102. https://doi.org/10.1167/iovs.10-7067.

61. Wang, Y., Sedimbi, S., Löfbom, L., Singh, A.K., Porcelli, S.A., and Cardell, S.L. (2018). Unique invariant natural killer T cells promote intestinal polyps by suppressing TH1 immunity and promoting regulatory T cells. Mucosal Immunol. *11*, 131–143. https://doi.org/10.1038/mi.2017.34.

62. Renukaradhya, G.J., Sriram, V., Du, W., Gervay-Hague, J., Van Kaer, L., and Brutkiewicz, R.R. (2006). Inhibition of antitumor immunity by invariant natural killer T cells in a T-cell lymphoma model in vivo. Int. J. Cancer *118*, 3045–3053. https://doi.org/10.1002/ijc.21764.

63. Sadegh, L., Chen, P.W., Brown, J.R., Han, Z., and Niederkorn, J.Y. (2015). NKT cells act through third party bone marrow-derived cells to suppress NK cell activity in the liver and exacerbate hepatic melanoma metastases. Int. J. Cancer *137*, 1085–1094. https://doi.org/10.1002/ijc.29480.

64. Wolf, M.J., Adili, A., Piotrowitz, K., Abdullah, Z., Boege, Y., Stemmer, K., Ringelhan, M., Simonavicius, N., Egger, M., Wohlleber, D., et al. (2014). Metabolic activation of intrahepatic CD8+ T cells and NKT cells causes nonalcoholic steatohepatitis and liver cancer via cross-talk with hepatocytes. Cancer Cell *26*, 549–564. https://doi.org/10.1016/j.ccell.2014.09.003.

65. Diao, H., Kon, S., Iwabuchi, K., Kimura, C., Morimoto, J., Ito, D., Segawa, T., Maeda, M., Hamuro, J., Nakayama, T., et al. (2004). Osteopontin as a Mediator of NKT Cell Function in T Cell-Mediated Liver Diseases. Immunity *21*, 539–550. https://doi.org/10.1016/j.immuni.2004.08.012.

66. Bedel, R., Matsuda, J.L., Brigl, M., White, J., Kappler, J., Marrack, P., and Gapin, L. (2012). Lower TCR repertoire diversity in Traj18-deficient mice. Nat. Immunol. *13*, 705–706. https://doi.org/10.1038/ni.2347.

67. Ren, Y., Sekine-Kondo, E., Shibata, R., Kato-Itoh, M., Umino, A., Yanagida, A., Satoh, M., Inoue, K., Yamaguchi, T., Mochida, K., et al. (2017). A Novel Mouse Model of iNKT Cell-deficiency Generated by CRISPR/Cas9 Reveals a Pathogenic Role of iNKT Cells in Metabolic Disease. Sci. Rep. *7*, 12765. https://doi.org/10.1038/s41598-017-12475-4.

68. Zhang, J., Bedel, R., Krovi, S.H., Tuttle, K.D., Zhang, B., Gross, J., Gapin, L., and Matsuda, J.L. (2016). Mutation of the Traj18 gene segment using TALENs to generate Natural Killer T cell deficient mice. Sci. Rep. *6*, 27375–27410. https://doi.org/10.1038/srep27375.

69. Chandra, S., Zhao, M., Budelsky, A., de Mingo Pulido, A., Day, J., Fu, Z., Siegel, L., Smith, D., and Kronenberg, M. (2015). A new mouse strain for the analysis of invariant NKT cell function. Nat. Immunol. *16*, 799–800. https://doi.org/10.1038/ni.3203.

70. Olszak, T., An, D., Zeissig, S., Vera, M.P., Richter, J., Franke, A., Glickman, J.N., Siebert, R., Baron, R.M., Kasper, D.L., and Blumberg, R.S. (2012). Microbial Exposure During Early Life Has Persistent Effects on Natural Killer T Cell Function. Science *336*, 489–493. https://doi.org/10.1126/science.1219328.

71. Ma, C., Han, M., Heinrich, B., Fu, Q., Zhang, Q., Sandhu, M., Agdashian, D., Terabe, M., Berzofsky, J.A., Fako, V., et al. (2018). Gut microbiome–mediated bile acid metabolism regulates liver cancer via NKT cells. Science *360*, eaan5931. https://doi.org/10.1126/science.aan5931.

72. Giannou, A.D., Kempski, J., Shiri, A.M., Lücke, J., Zhang, T., Zhao, L., Zazara, D.E., Cortesi, F., Riecken, K., Amezcua Vesely, M.C., et al. (2023). Tissue resident iNKT17 cells facilitate cancer cell extravasation in liver metastasis via interleukin-22 Tissue resident iNKT17 cells facilitate cancer cell extravasation in liver metastasis via interleukin-22. Immunity *56*, 125–142. https://doi.org/10.1016/j.immuni.2022.12.014.

73. Liu, Y., Munker, S., Müllenbach, R., and Weng, H.L. (2012). IL-13 signaling in liver fibrogenesis. Front. Immunol. *3*, 1–7. https://doi.org/10.3389/fimmu.2012.00116.

74. Bhattacharjee, S., Hamberger, F., Ravichandra, A., Miller, M., Nair, A., Affo, S., Filliol, A., Chin, L., Savage, T.M., Yin, D., et al. (2021). Tumor restriction by type I collagen opposes tumor-promoting effects of cancer-associated fibroblasts. J. Clin. Investig. *131*, e146987. https://doi.org/10.1172/JCI146987.

75. Mchedlidze, T., Waldner, M., Zopf, S., Walker, J., Rankin, A.L., Schuchmann, M., Voehringer, D., McKenzie, A.N.J., Neurath, M.F., Pflanz, S., and Wirtz, S. (2013). Interleukin-33-dependent innate lymphoid cells mediate hepatic fibrosis. Immunity *39*, 357–371. https://doi.org/10.1016/j.immuni.2013.07.018.

76. Gieseck, R.L., Ramalingam, T.R., Hart, K.M., Vannella, K.M., Cantu, D.A., Lu, W.-Y., Ferreira-González, S., Forbes, S.J., Vallier, L., and Wynn, T.A. (2016). Interleukin-13 Activates Distinct Cellular Pathways Leading to

Ductular Reaction, Steatosis, and Fibrosis. Immunity *45*, 145–158. https://doi.org/10.1016/j.immuni.2016.06.009.

77. Sonoda, K.-H., Exley, M., Snapper, S., Balk, S.P., and Stein-Streilein, J. (1999). Cd1-Reactive Natural Killer T Cells Are Required for Development of Systemic Tolerance through an Immune-Privileged Site. J. Exp. Med. *190*, 1215–1226. https://doi.org/10.1084/jem.190.9.1215.
78. Unutmaz, D., Xiang, W., Sunshine, M.J., Campbell, J., Butcher, E., and Littman, D.R. (2000). The Primate Lentiviral Receptor Bonzo/STRL33 Is Coordinately Regulated with CCR5 and Its Expression Pattern Is Conserved Between Human and Mouse. J. Immunol. *165*, 3284–3292. https://doi.org/10.4049/jimmunol.165.6.3284.
79. Madisen, L., Zwingman, T.A., Sunkin, S.M., Oh, S.W., Zariwala, H.A., Gu, H., Ng, L.L., Palmiter, R.D., Hawrylycz, M.J., Jones, A.R., et al. (2010). A robust and high-throughput Cre reporting and characterization system for the whole mouse brain. Nat. Neurosci. *13*, 133–140. https://doi.org/10.1038/nn.2467.
80. Narni-Mancinelli, E., Chaix, J., Fenis, A., Kerdiles, Y.M., Yessaad, N., Reynders, A., Gregoire, C., Luche, H., Ugolini, S., Tomasello, E., et al. (2011). Fate mapping analysis of lymphoid cells expressing the NKp46 cell surface receptor. Proc. Natl. Acad. Sci. USA *108*, 18324–18329. https://doi.org/10.1073/pnas.1112064108.
81. Reese, T.A., Liang, H.-E., Tager, A.M., Luster, A.D., Van Rooijen, N., Voehringer, D., and Locksley, R.M. (2007). Chitin induces accumulation in tissue of innate immune cells associated with allergy. Nature *447*, 92–96. https://doi.org/10.1038/nature05746.
82. Liang, H.-E., Reinhardt, R.L., Bando, J.K., Sullivan, B.M., Ho, I.-C., and Locksley, R.M. (2011). Divergent expression patterns of IL-4 and IL-13 define unique functions in allergic immunity. Nat. Immunol. *13*, 58–66. https://doi.org/10.1038/ni.2182.
83. Mombaerts, P., Iacomini, J., Johnson, R.S., Herrup, K., Tonegawa, S., and Papaioannou, V.E. (1992). RAG-1-deficient mice have no mature B and T lymphocytes. Cell *68*, 869–877. https://doi.org/10.1016/0092-8674(92)90030-G.
84. Mohrs, M., Shinkai, K., Mohrs, K., and Locksley, R.M. (2001). Analysis of Type 2 Immunity In Vivo with a Bicistronic IL-4 Reporter. Immunity *15*, 303–311. https://doi.org/10.1016/S1074-7613(01)00186-8.
85. O'Brien, M., Ernst, M., and Poh, A.R. (2023). An intrasplenic injection model of pancreatic cancer metastasis to the liver in mice. STAR Protoc. *4*, 102021. https://doi.org/10.1016/j.xpro.2022.102021.
86. Ducimetière, L., Lucchiari, G., Litscher, G., Nater, M., Heeb, L., Nuñez, N.G., Wyss, L., Burri, D., Vermeer, M., Gschwend, J., et al. (2021). Conventional NK cells and tissue-resident ILC1s join forces to control liver metastasis. Proc. Natl. Acad. Sci. *118*, e2026271118. https://doi.org/10.1073/pnas.2026271118.
87. Germain, P.-L., Lun, A., Garcia Meixide, C., Macnair, W., and Robinson, M.D. (2021). Doublet identification in single-cell sequencing data using scDblFinder. F1000Res. *10*, 979. https://doi.org/10.12688/f1000research.73600.1.
88. Hao, Y., Stuart, T., Kowalski, M.H., Choudhary, S., Hoffman, P., Hartman, A., Srivastava, A., Molla, G., Madad, S., Fernandez-Granda, C., and Satija, R. (2024). Dictionary learning for integrative, multimodal and scalable single-cell analysis. Nat. Biotechnol. *42*, 293–304. https://doi.org/10.1038/s41587-023-01767-y.

STAR★METHODS

KEY RESOURCES TABLE

REAGENT or RESOURCE	SOURCE	IDENTIFIER
Antibodies		
Rat Monoclonal CD16/32 (93)	Biolegend	101302; RRID: AB_312801
Rat Monoclonal Ly-6G (1A8) – Biotin	Biolegend	127604; RRID: AB_1186108
Rat Monoclonal CD19 (6D5) – Biotin	Biolegend	115504; RRID: AB_313639
Rat Monoclonal CD115 (AFS98) – Biotin	Biolegend	135508; RRID: AB_2085223
Rat Monoclonal F4/80 (BM8) – Biotin	Biolegend	123106; RRID: AB_893501
Hamster Monoclonal CD49a (HA31/8) – BUV395	BD	740262; RRID: AB_2740005
Rat Monoclonal CD45 (30-F11) – BUV496	BD	749889; RRID: AB_2874129
Streptavidin – BUV563	BD	612935; RRID: AB_2869708
Syrian Hamster Monoclonal KLRG1 (2F1) – BUV615	BD	751191; RRID: AB_2875213
Rat Monoclonal CD11b (M1/70) – BUV661	eBioscience	367-0112-82; RRID: AB_2869708
Armenian Hamster Monoclonal TCR beta (H57-597) – BUV737	eBioscience	367-5961-82; RRID: AB_2896026
Rat Monoclonal CD8a (53-6.7) – BUV805	eBioscience	368-0081-82; RRID: AB_2896078
Rat Monoclonal CXCR6 (SA05D1) – BV421	Biolegend	151109; RRID: AB_2616760
Rat Monoclonal CD49b (DX5) – Pacific Blue	Biolegend	108918; RRID: AB_2265144
Mouse Monoclonal NK-1.1 (PK136) – Pacific Blue	Biolegend	108722; RRID: AB_2132712
Rat Monoclonal CD117 (2B8) – Pacific Blue	Biolegend	105820; RRID: AB_493476
Mouse Monoclonal Ki-67 (B56) – BV480	BD	566109; RRID: AB_2739511
Rat Monoclonal CD62L (MEL-14) – BV570	Biolegend	104433; RRID: AB_10900262
Rat Monoclonal CD335 (29A1.4) – BV605	Biolegend	137619; RRID: AB_2562452
Rat Monoclonal CD19 (6D5) – BV605	Biolegend	115539; RRID: AB_11203538
Mouse Monoclonal T-bet (O4-46) – BV650	BD	564142; RRID: AB_2738616
Mouse Monoclonal NK-1.1 (PK136) – BV711	Biolegend	108745; RRID: AB_2563286
Rat Monoclonal CD4 (RM4-5) – Super Bright 780	eBioscience	78-0042-80; RRID: AB_2722967
Rat Monoclonal CD335 (29A1.4) – FITC	Biolegend	137606; RRID: AB_2298210
Mouse Recombinant Granzyme B (QA16A02) – PerCP/Cyanine5.5	Biolegend	372212; RRID: AB_2728379
Rat Monoclonal CD335 (29A1.4) – PerCP-eFluor 710	eBioscience	46-3351-82; RRID: AB_1834441
Armenian Hamster CD27 (LG.3A10) – PE	Biolegend	124210, RRID: AB_1236459
Rat Monoclonal CD8a (53-6.7) – PE	BD	553033; RRID: AB_394571
Rat Monoclonal I-A/I-E (M5/114.15.2) – PE	Biolegend	107607; RRID: AB_313322
Rat Monoclonal EOMES (Dann1mag) – PE-eFluor 610	eBioscience	61-4875-82; RRID: AB_2574614
Rat Monoclonal Siglec-F (E50-2440) – PE-CF594	BD	562757; RRID: AB_2687994
Armenian Hamster Monoclonal CD69 (H1.2F3) – PE-Cyanine5	eBioscience	15-0691-82; RRID: AB_468772
Armenian Hamster Monoclonal TCR beta (H57-597) PE – Cyanine5	Biolegend	109210; RRID: AB_313433
Rat Monoclonal CD274 (10F.9G2) – PE-Cyanine7	Biolegend	124314; RRID: AB_10643573
Rat Monoclonal Tim-4 (RMT4-54) – PE-Cyanine7	Biolegend	130010; RRID: AB_2565719
Streptavidin – PE-Cyanine7	Biolegend	405206; RRID: N/A
Mouse Monoclonal CD45.2 (104) – APC	Biolegend	109814; RRID: AB_389211
Mouse PBS-57 CD1d Tetramer – AF647	NIH Tetramer Core Facility	N/A
Mouse Unloaded CD1d Tetramer – AF647	NIH Tetramer Core Facility	N/A

(*Continued on next page*)

Continued

REAGENT or RESOURCE	SOURCE	IDENTIFIER
Rat Monoclonal CD90.2 (30-H12) – AF700	Biolegend	105320; RRID: AB_493725
Goat Polyclonal tdTomato/mCherry	SICGEN	AB8181-200; RRID: N/A
Rabbit Polyclonal tdTomato/mCherry	TaKaRa	632496; RRID: N/A
Goat Polyclonal GFP	SICGEN	AB0020-20; RRID: N/A
Mouse Alpha-Smooth Muscle Actin Monoclonal (1A4) – eFluor 660	eBioscience	50-9760-82; RRID: AB_2574362
Rat Monoclonal CD8a (4SM15) – PE	eBioscience	14-0808-82; RRID: AB_2572861
Donkey Anti-Goat Polyclonal IgG – AF594	Jackson ImmunoResearch	705-585-147; RRID: AB_2340433
Donkey Anti-Rabbit Polyclonal IgG – AF594	Jackson ImmunoResearch	711-585-152; RRID: AB_2340621
Donkey Anti-Goat Polyclonal IgG – AF488	Jackson ImmunoResearch	705-545-147; RRID: AB_2336933
Donkey Anti-Rat IgG Polyclonal IgG – AF647	Jackson ImmunoResearch	712-605-153; RRID: AB_2340694
Rat Monoclonal CD1d (20H2)	BioXCell	BE0179; RRID: AB_10949293
Rat Monoclonal NKG2D (CX5)	BioXCell	BE0334; RRID: AB_2894754
Rat Monoclonal Horseradish Peroxidase (HRPN)	BioXCell	BE0088; RRID: AB_1107775
Rat Monoclonal IL-4 (11B11)	BioXCell	BE0045; RRID: AB_1107707
Rat Monoclonal IL-13 (eBio1316H)	Invitrogen	16-7135-81; RRID: AB_763562
Chemicals, peptides, and recombinant proteins		
Zombie NIR Fixable Viability Kit	Biolegend	423106; RRID: N/A
DAPI	Invitrogen	D1306
Cultrex Reduced Growth Factor Basement Membrane Extract, Type 2, Pathclear	Bio-Techne	3533-005-002
Advanced DMEM/F-12	Gibco	12634-010
DMEM	Gibco	41966-029
DPBS	Gibco	14190144
Fetal Bovine Serum	Gibco	A5256701
N-Acetyl-L-cysteine 500mM (400X)	Sigma-Aldrich	A9165
N-2 Supplement (100X)	Gibco	17502048
B-27 Supplement (50X)	Gibco	17504-44
HEPES (1M)	Gibco	15630-056
Puromycin (10mg/ml)	InvivoGen	Ant-pr-1
Hygromycin B (50mg/ml)	Gibco	10687010
L-Glutamine (200mM)	Gibco	25030081
Penicillin-Streptomycin (10’000 U/ml;10 mg/ml)	Sigma-Aldrich	P4333
TrypLE Express Enzyme, no phenol red	Gibco	12604013
NutriFreez D10 Cryopreservation Medium	Sartorius	05-713-1E
Polyethylenimine (PEI)	Polysciences	23966-1
Polybrene Infection / Transfection Reagent	Sigma-Aldrich	TR-1003
G418	InvivoGen	ant-gn-1
RPMI 1640 medium	Gibco	21875034
Collagenase Type IV	Thermo Fisher Scientific	17104019
DNAse I	Roche	10104159001
GENEzol	Geneaid	GZR200
RNase Inhibitor	Applied Biosystems	N8080119
DNase I, RNase-free	Thermo Fisher Scientific	EN0521
Reaction Buffer with MgCl2 for DNase I	Thermo Fisher Scientific	B43
ProLong Diamond Antifade Mountant	Invitrogen	P36965
ImmEdge hydrophobic pen	Vector Laboratories	H-4000
Roti-Histofix 4 %	Carl Roth	P087.3
D(+)Saccharose	Carl Roth	9097.2

(*Continued on next page*)

Continued

REAGENT or RESOURCE	SOURCE	IDENTIFIER
Tissue-Tek O.C.T. Compound	Sakura Finetek	4583
Tissue-Tek Cryomold Standard	Sakura Finetek	4557
Bovine Serum Albumin (BSA) Fraction V, NZ-Origin	Carl Roth	8076.4
Ethanol absolute	VWR Chemicals	20821.321
Superfrost Plus Adhesion Microscope Slides	VWR	J1800AMNZ
Triton X-100	Sigma-Aldrich	X100
TWEEN 20	Sigma-Aldrich	P1379
Fast green FCF (C.I. 42053)	Sigma-Aldrich	F7258-25G
Direct Red 80	Sigma-Aldrich	365548-5G
Picric acid solution, saturated	Sigma-Aldrich	P6744-1GA
Acetic acid (glacial) 100% anhydrous	Sigma-Aldrich	1000631000
UltraClear	Biosystems	3905.9010PE
Eukitt Quick-hardening mounting medium	Sigma-Aldrich	03989
VivoGlo Luciferin, *In Vivo* Grade	Promega	P1043
Percoll	Sigma-Aldrich	GE17-0891-01
Critical commercial assays		
Quick-RNA MicroPrep Kit	Zymo Research	R1051
PowerUp SYBR Green Master Mix	Applied Biosystems	A25742
TaqMan Fast Advanced Master Mix	Applied Biosystems	4444557
BD Rhapsody Cartridge kit	BD	633733
BD Rhapsody Enhanced Cartridge Reagent Kit	BD	664887
BD Rhapsody cDNA kit	BD	633773
BD Rhapsody WTA amplification kit	BD	633801
Single-Cell Sample multiplexing kit	BD	633793
Foxp3 / Transcription Factor Staining Buffer Set	Invitrogen	00-5523-00
High-Capacity cDNA Reverse Transcription Kit	Applied Biosystems	4368813
Deposited data		
Single-cell RNA sequencing data	This paper	GEO: GSE274890
Experimental models: Cell lines		
APTKA	Provided by Florian Greten (Georg-Speyer-Haus, Germany)	N/A
APTKA-luc	This paper	N/A
APTKA-mCherry	This paper	N/A
MC-38	Provided by Mark Smyth (QIMR Berghofer Medical Research Institute, Australia)	N/A
MC38-luc	This paper	N/A
Experimental models: Organisms/Strains		
C57BL/6NRj	Janvier Labs	N/A
Cd1d $^{-/-}$: B6.129S6-Del(3Cd1d2-Cd1d1)1Sbp/J	The Jackson Laboratory	RRID: IMSR_JAX:008881
Traj18 $^{-/-}$: B6.Cg-Traj18<tm1.1Kro>/N	Provided by Paolo Dellabona (IRCCS, Italy)	N/A
Cxcr6 $^{Gfp/Gfp}$: B6.129P2-Cxcr6<tm1Litt>/J	The Jackson Laboratory	RRID: IMSR_JAX:005693
R26R $^{Ai14/Ai14}$: B6.Cg-Gt(ROSA) 26Sor<tm14(CAG-tdTomato)Hze>/J	The Jackson Laboratory	RRID: IMSR_JAX:007914
Ncr1 $^{Cre/wt}$ R26R $^{Ai14/wt}$: B6.Cg-Ncr1<tm1.1(icre)Viv> x B6.Cg-Gt(ROSA)26Sor<tm9(CAG-tdTomato)Hze>	Provided by Sonia Tugues (UZH, Switzerland)	N/A

(*Continued on next page*)

Continued

REAGENT or RESOURCE	SOURCE	IDENTIFIER
Lrat $^{Cre/wt}$ R26R $^{Ai14/Ai14}$: B6.Cg-Tg(Lrat-cre)1Rshw/Mmjax x B6.Cg-Gt(ROSA)26Sor<tm9(CAG-tdTomato)Hze>	Provided by Ingmar Mederacke (MHH, Germany)	MGI:5545650
Il4ra $^{fl/fl}$ *Il13* $^{Smart13/Smart13}$ *Arg1* $^{Yfp/Yfp}$: B6.C-Il4ra<tm2Fbb> x B6.129S4-Arg1<tm1Lky>/J x B6.129S4(C)-Il13<tm2.1Lky>/J	Provided by Christoph Schneider (UZH, Switzerland)	N/A
Rag1 $^{-/-}$: B6.129S7-Rag1<tm1Mom>/J	The Jackson Laboratory	RRID: IMSR_JAX:002216
Il4 $^{4Get/wt}$: B6.129-Il4<tm1Lky>/J	Provided by Manfred Kopf (ETHZ; Switzerland)	N/A
Oligonucleotides		
Il4 (Mm00445259_m1)	Thermo Fisher Scientific	4331182
Il13 (Mm00434204_m1)	Thermo Fisher Scientific	4331182
mCherry (Mr07319438_mr)	Thermo Fisher Scientific	4331182
Gapdh (Mm99999915_g1)	Thermo Fisher Scientific	4331182
Ifng (Mm01168134_m1)	Thermo Fisher Scientific	4331182
Tgfb1 (Mm01178820_m1)	Thermo Fisher Scientific	4331182
*Acta2*_fw: AGCCATCTTTCATTGGGATGG	This paper	N/A
*Acta2*_rv: CCCCTGACAGGACGTTGTTA	This paper	N/A
*Col1a1*_fw: GCTCCTCTTAGGGGCCACT	This paper	N/A
*Col1a1*_rv: CCACGTCTCACCATTGGGG	This paper	N/A
*Gapdh*_fw: TCGTGGATCTGACGTGCCGCCTG	This paper	N/A
*Gapdh*_rv: CACCACCCTGTTGCTGTAGCCGTAT	This paper	N/A
*Mult1*_fw: CACCTGTGTTTATGCAGATTGAT	This paper	N/A
*Mult1*_rv: TCTGAGATGCTGTCGGAAATTCA	This paper	N/A
*H60*_fw: GAGCCACCAGCAAGAGCAA	This paper	N/A
*H60*_rv: CCAGTATGGTCCCCAGATAGCT	This paper	N/A
Recombinant DNA		
pLenti PGK V5-LUC Neo (w623-2)	Addgene	21471; RRID: Addgene_21471
pLV-mCherry	Addgene	36084; RRID: Addgene_36084
pCMV-dR8.91	Provided by Christian Münz (UZH, Switzerland)	N/A
pMD2.G	Addgene	12259; RRID: Addgene_12259
Software and algorithms		
R v4.2.2	The R Foundation for Statistical Computing	https://www.r-project.org/
ImageJ2 v2.14.0	N/A	https://imagej.net/software/imagej2/
Rstudio v2023.03.0	Posit PBC	https://posit.co/download/rstudio-desktop/
Inform v2.6	PerkinElmer	https://www.akoyabio.com/phenoimager/inform-tissue-finder/
Phenochart v2.2.0	PerkinElmer	https://www.akoyabio.com/software-data-analysis/
FlowJo v10.9.0	FlowJo LLC	https://www.flowjo.com/
Other		
Injection syringe	Hamilton	7656-01
Hopkins Telescope	Karl Storz	64301AA
Intravascular catheter	BD	381337
Mucosal injection needle (33 gauge, small-hub RN needle, 45°, 400mm, point style 4)	Hamilton	7803-05
RN Nut	Hamilton	30902

(*Continued on next page*)

Continued

REAGENT or RESOURCE	SOURCE	IDENTIFIER
Camera control unit IMAGE1 S CONNECT	Karl Storz	TC200
Monitor	Karl Storz	9826NB
Camera Head	Karl Storz	TH102
Light cable	Karl Storz	495 FS
Light source	Karl Storz	20133720-1
Operating sheath	Karl Storz	61029D
Coated VICRYL Polyglactin 910	Ethicon	V303H
Wound clips 9 mm	Clay Adams	427631
Wound clip applier	Fine Science tools	12020-09
Lacryvisc ophtalmic ointment	Alcon	1857926
Insulin syringe 0.5 ml	B Braun	9151125S
70 μm Cell Strainers	Biologix	15-1070-2
UltraComp eBeads Plus Compensation Beads	Invitrogen	01-3333-42
FastPrep-24 homogenizer	MP Biomedicals	116004500
Zirconium oxide beads	Labgene Scientific	BER103BK
BD FACSAria III cell sorter	BD	N/A
BD FACSymphony S6 5L cell sorter	BD	N/A
Cytek Aurora 5L	Cytek Biosciences	N/A
LightCycler 480 II	Roche	05015278001
Vectra 3 Automated Quantitative Pathology Imaging System	PerkinElmer	N/A
IVIS Imaging System 200	PerkinElmer	N/A
Cryostar NX70 Cryostat	Epredia	15380755

EXPERIMENTAL MODEL AND STUDY PARTICIPANT DETAILS

Mice

C57BL/6NRj mice were purchased from Janvier Labs. *Cd1d* $^{-/-}$ mice[77] and *Cxcr6* $^{Gfp/Gfp}$ mice[78] were purchased from The Jackson Laboratory. *Traj18* $^{-/-}$ mice[69] were provided by Paolo Dellabona (IRCCS, Italy). R26R $^{Ai14/Ai14}$ mice[79] were provided by Melanie Greter (UZH, Switzerland). *Ncr1* $^{Cre/wt}$ R26R $^{Ai14/wt}$ mice[80] were provided by Sonia Tugues (UZH, Switzerland). *Ncr1* $^{Cre/wt}$ R26R $^{Ai14/wt}$ were crossed to *Cxcr6* $^{Gfp/Gfp}$ mice to obtain *Ncr1* $^{Cre/wt}$ R26R $^{Ai14/wt}$ *Cxcr6* $^{Gfp/wt}$ (*Ncr1* ^{Tdtomato} *Cxcr6* ^{Gfp}) mice. *Lrat* $^{Cre/wt}$ R26R $^{Ai14/Ai14}$ mice[11] were provided by Ingmar Mederacke (MHH, Germany). *Il4ra* $^{fl/fl}$ *Il13* $^{Smart13/Smart13}$ *Arg1* $^{Yfp/Yfp}$ mice[53,81,82] were crossed to *Lrat* $^{Cre/wt}$ R26R $^{Ai14/Ai14}$ mice to obtain *Lrat* $^{Cre/wt}$ *Il4ra* $^{fl/fl}$ mice. *Lrat* $^{Cre/wt}$ *Il4ra* $^{fl/fl}$ mice were used for the selective deletion of *Il4ra* in hepatic stellate cells. Cre-negative littermates were used as control. *Rag1* $^{-/-}$ mice[83] were provided by Burkhard Becher (UZH, Switzerland). *Il4* $^{4Get/wt}$ mice[84] were provided by Manfred Kopf (ETHZ, Switzerland).

All strains have a C57BL/6 background. Eight-to-twelve-week-old mice of either sex were used with equal age- and sex-distribution among experimental groups. Breeding and experiments were performed under specific pathogen-free (SPF) conditions in facilities of the Laboratory Animal Services Center (LASC) at the University of Zurich. Mice had access to food and water *ad libitum* and were kept in a 12-hour light/dark cycle. All mouse experiments were performed according to Swiss cantonal and federal regulations on animal protection and approved by the Swiss Cantonal Veterinary Office (license numbers 156/2018 and 031/2021).

Organoids and cancer cell lines

APTKA organoids were provided by Florian Greten (Georg-Speyer-Haus, Germany). The MC38 cell line was originally provided by Mark Smyth (QIMR Berghofer Medical Research Institute, Australia). Cell lines were not authenticated. Cells were tested negative for Mycoplasma ssp. by PCR analysis. Cells were also tested negative for 18 additional mouse pathogens by PCR (IMPACT II Test, IDEXX Bioanalytics).

Organoids and cancer cells were cultured at 37°C in a humid atmosphere with 5% CO_2. APTKA organoids were embedded in Basement Matrix Extract type 2 (BME, Bio-Techne) and cultured with organoid medium, consisting of Advanced DMEM/F-12 (Gibco), supplemented with 10 mM HEPES (Gibco), 100 U/ml Penicillin, 100 μg/ml Streptomycin (Sigma-Aldrich), 2 mM

L-Glutamine (Gibco), 1.25 mM N-Acetyl-L-cysteine (Sigma-Aldrich), 1% N-2 and 2% B-27 supplements (Gibco). MC38 cells were cultured in DMEM (Gibco) supplemented with 10% fetal bovine serum (Gibco), 100 U/ml Penicillin, 100 μg/ml Streptomycin (Sigma-Aldrich) and 2 mM L-Glutamine (Gibco).

mCherry-expressing APTKA (APTKA-mCherry), luciferase-expressing MC38 (MC38-luc), and luciferase-expressing APTKA (APTKA-luc) organoids were generated by lentiviral transduction using 8 μg/ml polybrene (Sigma-Aldrich). Lentiviruses were produced by co-transfection of the respective lentiviral expression vector pLV-mCherry (Addgene #36084) and pLenti PGK V5-LUC Neo (Addgene #21471) and the viral packaging envelope plasmids pMD2g (Addgene #12259) and pCMV-dR8.91 (provided by Christian Münz, UZH, Switzerland) into 293T cells (ATCC, CRL-3216). A DNA:polyethylenimine (Polysciences) μg ratio of 1:3 was used for transfection. mCherry$^+$ cells were sorted by Fluorescence-Activated Cell Sorting (FACS). Luciferase-expressing MC38 and APTKA cells were selected with 500 μg/ml G418 (InvivoGen) for 10 days. Clonal selection was then performed for all cell and organoid lines.

METHOD DETAILS

Collection and expansion of APTKA organoids

Cryopreserved organoids were thawed and seeded in 4 domes of BME (75 μl each) on 6-well plates and transferred to a 37°C cell culture incubator. Once the BME was polymerized, 3 ml of organoid medium were added to each well. To collect organoids for passaging or injection, the medium was aspirated. One ml of ice-cold PBS was added per seeded well. The domes from each well were mechanically disrupted using a bent 1-ml pipette tip, and organoids were transferred into a 15-ml tube containing 10 ml of ice-cold PBS. The organoids were then centrifuged for 5 minutes at 290 g, and the supernatant was aspirated. The cell pellet was resuspended with a 200-μl bent pipette tip in 0.5 ml of ice-cold PBS to dissociate the organoids. Ten ml of ice-cold PBS was then added. The cells were centrifuged for 5 minutes at 290 g and the supernatant was aspirated. For further culture, dissociated APTKA organoids were resuspended in BME.

Orthotopic injection of APTKA organoids

Orthotopic injection of organoids was performed as described.[31] Following harvesting as outlined above, two domes (approximately 1.5 x 10^5 cells) of APTKA or APTKA-mCherry organoids were resuspended in 70 μl PBS. Mice were anesthetized and transferred onto a warming pad set at 37°C. Ophthalmic ointment (Alcon) was applied to the eyes to prevent drying. The colon was cleaned with a rapid enema with 5-10 ml PBS pre-warmed to 30°C using the plastic tubing of a 20G x 48 mm intravascular catheter (BD) attached to a 20-ml syringe (B Braun). Organoids were injected into the distal colon mucosa by colonoscopy-guided mucosal injection with a custom injection needle (Hamilton).

MC38 cells were not used in the orthotopic model due to the failure to form a primary colon tumor. Metastatic nodules were counted using a stereotactic microscope.

Intrasplenic injection of APTKA organoids or MC38 cells

Intrasplenic injection of APTKA organoids or MC38 cells was performed as described.[85,86] 1.5 x 10^5 cells from dissociated APTKA-luc or APTKA-mCherry organoids or 5 x 10^5 MC38-luc cells were resuspended in 50 μl PBS. Pre-emptive analgesia (0.04 mg/kg fentanyl and 0.1 mg/kg buprenorphine) was administered by intraperitoneal injection. Mice were anesthetized and transferred onto a warming pad set at 37°C. Ophthalmic ointment (Alcon) was applied to the eyes to prevent drying. The mice were placed in a lateral position on the right side. The fur along the torso was shaved, and the skin was scrubbed with a sterile pad wetted with 70% ethanol. A single 1-cm incision was made in the left upper abdominal wall to access the peritoneal cavity, and the spleen was exposed on a sterile gaze using surgical forceps. APTKA organoids or MC38 cells were injected into the spleen using a 0.5-ml U-100 insulin syringe with a 30G x 8 mm needle. After 15 seconds, the needle was retracted, and the injection site was compressed using a sterile gauze. After 3 minutes, the splenic artery and vein were ligated near the hilum with 2 stitches each using a surgical needle holder and absorbable coated polyglactin sutures (Ethicon). Immediately thereafter, the spleen was resected. The peritoneal wall was sutured with 3 stitches and the skin was closed with wound clips (Clay Adams). Mice received buprenorphine (0.01 mg/ml) *ad libitum* for 48 hours after surgery. Metastases were visualized and quantified using an IVIS 200 imaging system (PerkinElmer).

Ex vivo bioluminescence

APTKA-luc- and MC38-luc-derived metastases were visualized and quantified using an IVIS 200 imaging system (PerkinElmer) 20 minutes after intraperitoneal injection (i.p.) of 150 mg/kg D-Luciferin in PBS (Promega).

Injection of monoclonal antibodies

To block CD1d, mice were injected i.p. with anti-mouse CD1d (100 μg/mouse; BioXCell) in 100 μL of PBS immediately after organoid injection and then twice weekly. Control mice received 100 μL of PBS on the same schedule. For cytokine blockade, anti-mouse IL-4 (500 μg/mouse; BioXCell) or anti-mouse IL-13 (200 μg/mouse; Invitrogen) was injected i.p. in 100 μL or 200 μL of PBS, respectively, 1 hour before organoid injection. To block NKG2D, mice were injected i.p. with anti-mouse NKG2D (500 μg/mouse; BioXCell) in 100 μL of PBS, 1 hour before organoid injection. Anti-HRPN (500 μg/mouse; BioXCell) served as the isotype control for IL-4, IL-13, and NKG2D blockade.

Sorting of NKT cells

Livers were digested into a single-cell suspension. Lymphocyte enrichment was performed using a density gradient centrifugation step (Percoll, Sigma-Aldrich). The gating strategy did not include staining for TCR-β or the use of CD1d tetramer loaded with PBS57 (an α-GalCer analog) to prevent potential transcriptional changes induced by the interaction of the TCR. Instead, NKT cells were sorted as single, live, $CD45^+$, $Ly6G^-$, $CD19^-$, $CD115^-$, F4/80^-, $CXCR6^+$, $CD8^-$, $NK1.1^+$ $NKp46^-$ cells using a FACSAria III (BD) or a FACSymphony S6 5L (BD) cell sorter.

qRT-PCR

Fifty mg of liver tissue was homogenized in GENEzol Reagent (Geneaid) using zirconium oxide beads (Labgene Scientific) and a FastPrep tissue homogenizer (MP Biomedicals). Total RNA was isolated by phenol-chloroform extraction following the manufacturer's instructions. 2 units of DNAse I (Thermo Fisher Scientific) per 10 μg of template RNA were used to digest genomic DNA.

RNA was extracted from sorted NKT cells using a Quick-RNA Microprep Kit (Zymo Research) following the manufacturer's instructions.

Total RNA was reverse transcribed using a high-capacity cDNA reverse transcription kit (Applied Biosystems). Real-time quantitative PCR was performed using PowerUp SYBR Green (Applied Biosystems) or TaqMan Fast Advanced Master Mix (Applied Biosystems). *Gapdh* was used as an internal reference gene, and the relative expression of target genes was calculated as $2^{-\Delta Ct}$.

Flow cytometry

Livers were harvested in RPMI supplemented with 10% FCS and digested with collagenase IV (1 mg/ml, Thermo Fisher Scientific) and DNase I (50 μg/ml, Roche) for 45 minutes at 37°C on a rotating device. Cells were washed with PBS containing 2 mM EDTA and filtered through a 70-μm strainer (Biologix). Red blood cells were lysed using a red blood cell lysis buffer (17 mM Tris pH 7.2, 144 mM NH_4Cl) for 2 minutes and cells were washed with PBS. Following 10 minutes of incubation with anti-CD16/32 in PBS containing 2 mM EDTA, single-cell suspensions were stained for surface molecules in 50 μl antibody mix in PBS containing 2 mM EDTA for 30 minutes at 4°C. For CD1d tetramer staining, CD1d-PBS57 or CD1d-unloaded was added to the surface antibody mix and cells were stained for 15 minutes at room temperature and then 30 minutes at 4°C. For intracellular staining, cells were fixed and permeabilized for 40 minutes at 4°C using the Foxp3/Transcription Factor Staining Buffer Set (Invitrogen). Single-cell suspensions were then stained for intracellular molecules in permeabilization buffer overnight at 4°C. Samples were washed once with permeabilization buffer and once with PBS 2mM EDTA and were acquired using a Cytek Aurora spectral flow cytometer 5L.

Immunofluorescence

Livers were fixed in 4% formaldehyde (Carl Roth) for 4 hours at room temperature and subsequently dehydrated in 15%, followed by 30% sucrose (Carl Roth) in PBS for 24 hours in each solution at 4 °C. Livers were then embedded and frozen in O.C.T. (Sakura), and 10-μm cryosections were cut using a cryotome. Sections were dried for 30 minutes at 37 °C, washed with PBS, and then blocked and permeabilized with PBS containing 4% bovine serum albumin (Carl Roth) and 0.1% Triton X-100 (Sigma-Aldrich) at room temperature for 10 minutes. Slides were then washed with PBS containing 0.05% Tween 20 (Sigma-Aldrich) and stained with a primary antibody in PBS containing 1% BSA at 4 °C overnight. Next, slides were washed and stained with a secondary antibody mix in PBS 1% BSA. Finally, slides were washed and incubated with 0.5 μg/ml DAPI (Invitrogen) for 5 minutes and mounted with Prolong Diamond medium (Invitrogen). Stained slides were scanned using the automated multispectral microscopy system Vectra 3.0 (PerkinElmer). Spectral unmixing was performed using inForm software v2.6 (PerkinElmer).

Sirius red staining

Livers were fixed, dehydrated, frozen, and sectioned as previously described in the "immunofluorescence" section. Frozen liver sections were dried for 30 minutes at 37°C and fixed in Kahle fixative (4% Formaldehyde, 0.02% acetic acid, and 28% ethanol in distilled H_2O) for 10 minutes at room temperature. The fixed sections were washed in distilled H_2O and then incubated in 0.04% Fast Green (Sigma-Aldrich) for 15 minutes at room temperature. The sections were then washed in distilled H_2O and stained with 0.1% Fast Green and 0.04% Sirius Red (Sigma-Aldrich) in saturated picric acid (Sigma-Aldrich) for 30 minutes at room temperature. Sections were washed 2 times for 5 minutes in 0.5% glacial acetic acid (Sigma-Aldrich). Tissue sections were dehydrated through an ethanol series (70%, 80%, 96%, and 100% ethanol, 30 seconds each) and cleared in Ultraclear (Biosystems) for 2 minutes. Slides were mounted with Eukitt mounting medium (Sigma-Aldrich) and stored at room temperature protected from light. Stained slides were scanned using the automated multispectral microscopy system Vectra 3.0 (PerkinElmer). Tissue segmentation and quantification of Sirius red-positive area was performed on twenty images (20 x magnification) per liver and analyzed using inForm software v2.6 (PerkinElmer).

Single-cell RNA sequencing

Single-cell suspensions were prepared from individual liver samples (n = 5 per condition). Cells were labeled using the BD Single-Cell Multiplexing Kit and pooled according to their respective conditions. Liver NKT cells were isolated using a BD FACSAria III cell sorter as single, live, $CD45^+$, $CD115^-$, F4/80^-, $CD19^-$, $Ly6G^-$, $CXCR6^+$, $CD8^-$, $NK1.1^+$, $NKp46^-$ cells. 40'000 cells were loaded onto a BD Rhapsody cartridge and processed for cDNA synthesis according to the BD Rhapsody Single-Cell Capture and cDNA Synthesis

protocol (Doc ID: 23-22951(01)). Library amplification was then carried out following the BD Rhapsody System mRNA Whole Transcriptome Analysis (WTA) and Sample Tag Library Preparation Protocol (Doc ID: 23-24119 (02)). Sequencing was conducted on an Illumina NovaSeq X Plus platform using 150 bp paired-end reads (R1 = 51 cycles, R2 = 71 cycles), achieving an average sequencing depth of approximately 50,000 reads per cell. Read alignment, cell barcode demultiplexing, deduplication of reads, generation of expression matrices, and quality report were performed using the Rhapsody Sequence Analysis Pipeline v2.0.

The expression matrices were further analyzed in R v4.2.2. Cells were filtered to exclude those with more than 10% mitochondrial content and less than 2% ribosomal protein content. Duplicate cells were removed using scDblFinder.[87] The Seurat pipeline v5 was employed for normalization, dimensionality reduction, and clustering of the expression data.[88] Gene set enrichment analysis was conducted using the UCell algorithm via the escape R package v1.99.[43,44]

QUANTIFICATION AND STATISTICAL ANALYSIS

Statistical significance was calculated with one-way analysis of variance (ANOVA) with Dunn's multiple comparisons correction when comparing the means of three or more independent groups. Two-way ANOVA was employed to examine the interaction between two independent variables on a dependent variable. Fisher's Least Significant Difference (LSD) post-hoc test was used for pairwise comparisons between group means. Mann-Whitney two-tailed U tests were applied to compare the medians of two independent groups. $p < 0.05$ was considered significant ($^{*}p < 0.05$, $^{**}p < 0.01$, $^{***}p < 0.001$, and $^{****}p < 0.0001$). Statistical analysis was performed using GraphPad statistical software v10.2.0 (GraphPad Software Inc.).